

Exact Resummations in the Theory of Hydrodynamic Turbulence:

0. Line-Resummed Diagrammatic Perturbation Approach

Victor L'vov* and Itamar Procaccia†

*Departments of * Physics of Complex Systems and † Chemical Physics,*

The Weizmann Institute of Science, Rehovot 76100, Israel,

**Institute of Automation and Electrometry, Ac. Sci. of Russia, 630090, Novosibirsk, Russia*

Abstract

The lectures presented by one of us (IP) at the Les Houches summer school dealt with the scaling properties of high Reynolds number turbulence in fluid flows. The results presented are available in the literature and there is no real need to reproduce them here. Quite on the contrary, some of the basic tools of the field and theoretical techniques are not available in a pedagogical format, and it seems worthwhile to present them here for the benefit of the interested student. We begin with a detailed exposition of the naive perturbation theory for the ensemble averages of hydrodynamic observables (the mean velocity, the response functions and the correlation functions). The effective expansion parameter in such a theory is the Reynolds number (Re); one needs therefore to perform infinite resummations to change the effective expansion parameter. We present in detail the Dyson-Wyld line resummation which allows one to dress the propagators, and to change the effective expansion parameter from Re to $O(1)$. Next we develop the “dressed vertex” representation of the diagrammatic series. Lastly we discuss in full detail the path-integral formulation of the statistical theory of turbulence, and show that it is equivalent order by order to the Dyson-Wyld theory. On the basis of the material presented here one can proceed smoothly to read the recent developments in this field.

1. INTRODUCTION

The exact description of fluid flows is provided by the specification of the velocity field $\mathbf{u}(\mathbf{r}, t)$ as a function of space and time. Such a description is natural for “laminar” flows of fluids whose velocity field is not strongly fluctuating in space and time. On the other hand, for “turbulent” flows, which are states of fluids whose velocity field $\mathbf{u}(\mathbf{r}, t)$ appears highly erratic as a function of \mathbf{r} and t , it is more sensible to consider a statistical description. The statistical description is particularly useful in situations where the flow is driven by stationary external agents. Examples of such stationary driving mechanisms are found in shear turbulence, grid turbulence, convective turbulence, etc. It is believed that in such flows it makes sense to consider long time averages of functions of the velocity field $\mathbf{u}(\mathbf{r}, t)$. For example, if the driving is arranged such that the fluid as a whole is confined in some volume V , the mean velocity must vanish:

$$\langle \mathbf{u}(\mathbf{r}, t) \rangle \equiv \frac{1}{V} \int d\mathbf{r} \lim_{T \rightarrow \infty} \frac{1}{2T} \int_{-T}^T \mathbf{u}(\mathbf{r}, t) dt = 0 . \quad (1.1)$$

The pointed brackets indicate here an average with respect to space and time. Likewise, correlation functions can be defined:

$$\begin{aligned} & \langle \mathbf{u}(\mathbf{r} + \mathbf{r}', t + \tau) \mathbf{u}(\mathbf{r}, t) \rangle \\ & \equiv \frac{1}{V} \int d\mathbf{r} \lim_{T \rightarrow \infty} \frac{1}{2T} \int_{-T}^T \mathbf{u}(\mathbf{r} + \mathbf{r}', t + \tau) \mathbf{u}(\mathbf{r}, t) dt . \end{aligned} \quad (1.2)$$

If the state of the fluid is statistically homogenous in space and time, the averaging process (1.2) results in a function of \mathbf{r}' and τ only.

One of the most important open problems of statistical physics is whether the statistical description of turbulence displays universal characteristics. Many important concepts were developed in the attempt to answer this question. It was recognized by Richardson [1,2] in the ‘20’s that quantities which depend on one space point have no chance to claim universality. The velocity field $\mathbf{u}(\mathbf{r}, t)$ and all its functions are fatally sensitive to the large scale components which are introduced by the external driving agents. In this picture the driving acts on the large scales, leading to maximally large velocity fluctuations on the macroscale L , which is known as the “outer” scale of turbulence. The typical scale of the velocity fluctuations is denoted as U_L . The order of magnitude of $\mathbf{u}(\mathbf{r}, t)$ at every \mathbf{r} is about U_L . Richardson suggested that the quantities that may have universal aspects are the velocity *differences* $\delta \mathbf{u}(\mathbf{r} + \mathbf{R}, \mathbf{r}, t) \equiv \mathbf{u}(\mathbf{r} + \mathbf{R}, t) - \mathbf{u}(\mathbf{r}, t)$. In taking differences one eliminates the contribution of the large scale motion, and may hope to see universal properties that are independent of

the driving mechanism. It was one of the main suggestions of Kolmogorov that for R that is much smaller than L and much larger than a “dissipative” scale η , statistical averages of functions of $\delta\mathbf{u}(\mathbf{r} + \mathbf{R}, \mathbf{r}, t)$ may show universality. The dissipative scale η depends on the kinematic viscosity of the fluid ν , and on the single most important dimensionless number in the theory of turbulence, i.e. the Reynolds number Re . This number is defined as [3]

$$Re = \frac{U_L L}{\nu}, \quad (1.3)$$

and in the Kolmogorov approach it is asserted that $\eta/L \sim Re^{-3/4}$. In other words, as $Re \rightarrow \infty$ there is a larger and larger range of scales R for which functions of $\delta\mathbf{u}(\mathbf{r} + \mathbf{R}, \mathbf{r})$ are expected to show universal properties.

In most experimental applications it is customary to consider the longitudinal component of $\delta\mathbf{u}(\mathbf{r} + \mathbf{R}, \mathbf{r}, t)$ only:

$$\delta u(\mathbf{r} + \mathbf{R}, \mathbf{r}, t) \equiv \delta\mathbf{u}(\mathbf{r} + \mathbf{R}, \mathbf{r}, t) \cdot \frac{\mathbf{R}}{R}. \quad (1.4)$$

The essence of the Kolmogorov approach to the issue of universality in turbulence, which was suggested in 1941 [4] (K41) is that it is possible to construct a local theory with one universal scaling exponent. This universal exponent was ascribed to $\delta u(\mathbf{r} + \mathbf{R}, \mathbf{r})$, stating that

$$\delta u(\mathbf{r} + \mathbf{R}, \mathbf{r}) \sim R^{1/3}. \quad (1.5)$$

It was asserted that $\delta u(\mathbf{r} + \mathbf{R}, \mathbf{r})$ is the only scaling field that has to be considered, in the sense that the structure functions $S_n(R)$ which can be formed from $\delta u(\mathbf{r} + \mathbf{R}, \mathbf{r}, t)$ satisfy the scaling laws

$$\begin{aligned} S_n(R) &\equiv \langle\langle [\delta u(\mathbf{r} + \mathbf{R}, \mathbf{r}, t)]^n \rangle\rangle \\ &\sim (\bar{\varepsilon} R)^{n\zeta_n} \sim (\bar{\varepsilon} R)^{n/3} \end{aligned} \quad (1.6)$$

for values of R in the “inertial range” $L \gg R \gg \eta$. In (1.6) $\bar{\varepsilon}$ is the mean (really in the double bracketed sense of (1.1) but defined by an overbar to save notation) of the dissipation field $\varepsilon(\mathbf{r}, t)$,

$$\varepsilon(\mathbf{r}, t) \equiv \frac{\nu}{2} [\partial_\alpha u_\beta(\mathbf{r}, t) + \partial_\beta u_\alpha(\mathbf{r}, t)]^2. \quad (1.7)$$

This suggestion of Kolmogorov was immediately attacked both by theorists (e.g. Landau) and experimentalists (for a recent review see e.g. [5]). Indeed, it is rather astonishing

that a problem like fluid turbulence, which suffers from very large fluctuations and strong correlations, should be amenable to such a simple description; even Kolmogorov himself revised his thinking and changed (1.6) to a more complicated form (which fell under attack as well). Indeed, one measurement that raised a lot of objections to the K41 approach is the measurement of the correlation function of the dissipation field $K_{\varepsilon\varepsilon}(r)$

$$K_{\varepsilon\varepsilon}(R) = \langle \hat{\varepsilon}(\mathbf{r} + \mathbf{R}, t) \hat{\varepsilon}(\mathbf{r}, t) \rangle \sim R^{-\mu} . \quad (1.8)$$

where $\hat{\varepsilon}(\mathbf{r}, t) = \varepsilon(\mathbf{r}, t) - \bar{\varepsilon}$. It was found in experiments that $K_{\varepsilon\varepsilon}(R)$ decays very slowly in the inertial range, with μ having a numerical value in the range 0.20-0.25 [6]. It was claimed that the K41 theory required μ to vanish. Accordingly, there have been many attempts to construct models of turbulence to take (1.8) into account and to explain how the measured deviations ($\zeta_n - 1/3$) in the exponents of the structure functions were related to μ .

Our aim is to present a Navier-Stokes based theory of turbulence. This theory attempts to study the universality of turbulence on scales belonging to the bulk of the inertial range using the equations of fluid mechanics. We are not going to review the variety of phenomenological *ad hoc* models which have proliferated in recent years. It is our belief that recent progress in the analytic theory brings us a long way towards understanding the scaling properties of turbulence, and it is important at this point to examine carefully what is known, to separate false starts from genuine progress, and to delineate the domain of firm results. In doing so we will also attempt to carefully assess the main open problems that await further research.

The equations of fluid mechanics are partial differential equations, and it is natural to consider them as a classical field theory, and to attempt to apply techniques of perturbation theory and renormalization that found spectacular success in the context of quantum field theory. Indeed, such attempts were made with the help of various closure procedures like Kraichnan's Direct Interaction Approximation [7] and many others (for review of different closure schemes see, e.g. [8]). A more systematic approach was suggested to be found within diagrammatic perturbation approaches for non-equilibrium processes like the Wyld diagrammatic technique [9] for the Navier-Stokes equation. Generalizations of the Wyld diagrammatic technique were suggested by Martin, Siggia, Rose [10] and by Zakharov and L'vov [11].

In performing such calculations one faces several serious difficulties. Firstly, turbulence has no small parameter. The naive perturbation expansion of the Navier-Stokes equations results in increasing powers of the Reynolds number, and this is rather inconvenient in a situation where one is interested in the limit $\text{Re} \gg 1$. Wyld [9] found a way to overcome this

difficulty; by performing line renormalization like Dyson's quantum field analog one finds a perturbative theory in which the coupling parameter is of $O(1)$. This is an important step, but it does not save Wyld's theory from severe problems. The main problem of the Wyld theory is that it is written in terms of the correlation functions of the field $\mathbf{u}(\mathbf{r}, t)$ itself. As mentioned above, such quantities are not universal, and they are dominated by large scale contributions. In addition, functions of $\mathbf{u}(\mathbf{r}, t)$ itself are not Galilean invariant. Wyld attempted therefore to work in terms of Fourier transforms of these quantities. Indeed, the correlation functions in \mathbf{k}, ω representation are expected to be universal in the regime $1/\eta \gg k \gg 1/L$. Unfortunately, the theory in \mathbf{k}, ω representation involves integrals over the whole \mathbf{k}, ω range, and the theory picks up infra-red divergences that cannot be eliminated easily.

Kraichnan has suggested that a theory that does not suffer from the problems of Wyld's expansion can be formulated in Lagrangian coordinates [12,13]. From the point of view of developing the theory in terms of universal quantities this suggestion was correct. Unfortunately the perturbation theory which is based on the Lagrangian representation is not of the diagrammatic type, and higher order terms with its coefficients cannot be found simply on the basis of topological features of the diagrams. We shall not be interested here in theories that contain arbitrary truncations. Such theories are uncontrolled, and it is our hope that one can achieve a fully controlled theory of turbulence. We seek therefore a formulation that lends itself to a diagrammatic description and which comes as close as possible to using as building blocks functions of $\delta u(\mathbf{r} + \mathbf{R}, \mathbf{r})$. A theory that has all the right ingredients was formulated by Belinicher and L'vov [14] (see also [15]). This theory went under the name "quasi-Lagrangian"; this name turned out to be unfortunate, since it left the impression of an approximate theory. Recently [16] we revisited this theory and reiterated that it is not an approximate theory, but rather an exact renormalization scheme that differs from the Wyld technique.

The aim of these notes is to review the basic tools of the field theoretic diagrammatic approach to the Navier-Stokes problem. There are essentially no new developments in these notes, but they are meant to bring the student to a level of expertise that would allow a smooth entry into the latest developments. We develop in full detail the naive perturbation theory (sec.2) for the Green's function and the 2-point correlation function. This theory is badly diverging in powers of Re . In sec.3 we discuss the line resummation which results in the Dyson equation for the Green's function and the Wyld equation for the correlator. In these equations, which are also presented as infinite diagrammatic series expansions, the

effective coupling constant is of $O(1)$. We discuss briefly 3-point and higher order correlation functions, and in Sect. 4 we turn to the functional integral formulation of the renormalized perturbation theory. We show in detail that the diagrammatic expansion obtained in this formulation is identical, order by order, with the Wyld formulation, and that either one can be used at will [10,17,18]. The interested student is invited then to continue reading Refs. [16,19,20] in which the Belinicher-L'vov renormalization scheme is used to develop a consistent theory of normal and anomalous scaling in turbulence.

2. NAIVE PERTURBATION THEORY

A. Introduction

As was mentioned in section 1, we are mostly interested in the calculation of averages and correlation functions, which are obtained in the long time limit of the *forced* Navier-Stokes equations. Since the equations contain a viscous damping, it is assumed that the balance between forcing and damping leads after a time to stationary statistics which are independent of the initial conditions. Roughly speaking the picture is of a nonlinear problem that generates its own ergodic measure, and the forcing is chosen such that the ergodic measure (at least as far as the calculated quantities are concerned) is a property of the Navier-Stokes equations and not of the forcing. In other words, the solution roams forever on a strange attractor, and the forcing is used mainly to keep the system away from the (stable) zero solution, but without ruining too much the measure on the attractor.

In our formal scheme we will expand ergodic averages for the nonlinear problem in terms of averages of solutions of the linear problem (i.e with the nonlinearity discarded). Not surprisingly, since the measure of the nonlinear problem is *very* different from the measure of the linear problem, we will see that our expansion has very miserable convergence properties. Actually the naive expansion diverges, and it cannot be truncated at any order. It has meaning only for the series as a whole. Nevertheless, one can perform infinite partial resummations of this series to achieve a new series that has somewhat better properties, i.e. the terms remain all of the same order. We stress right at the beginning that many of our steps have dubious mathematical validity, and the fact that they are common practice in many field theories cannot be really taken as an excuse. At least we will not hide the difficulties.

The Eulerian velocity field is denoted in our discussion as $\mathbf{u}(\mathbf{r}, t)$. In later notation we

shall sometimes use the 4-vector notation $\mathbf{u}(x)$, where $x \equiv (\mathbf{r}, t)$. In the mathematical literature it is customary to write the Navier-Stokes equations as an initial value problem without any type of forcing:

$$\frac{\partial \mathbf{u}}{\partial t} + (\mathbf{u} \cdot \nabla) \mathbf{u} - \nu \nabla^2 \mathbf{u} - \nabla p = 0, \quad \nabla \cdot \mathbf{u} = 0. \quad (2.1)$$

For the physicist the equations of fluid mechanics are a projection onto a set of slow variables of the many-body microscopic dynamics. In such a projection, when successful, the host of irrelevant degrees of freedom remain in the form of a “noise” term in the equation of motion of the slow variables. The basic assertion is that the irrelevant degrees of freedom are much faster, and reach local equilibrium on a short time scale which is irrelevant for the hydrodynamic description. Thus, the physicist writes Eq. (2.1) in the form

$$\partial \mathbf{u} / \partial t + (\mathbf{u} \cdot \nabla) \mathbf{u} - \nu \nabla^2 \mathbf{u} - \nabla p = \mathbf{f}, \quad (2.2)$$

where the fluctuation dissipation theorem dictates that the two-point correlation function of the “random” force \mathbf{f} is related to the viscosity and the temperature of the fluid:

$$\overline{f_\alpha(\mathbf{r}, t) f_\beta(\mathbf{r}', t')} = 2\nu T \delta(\mathbf{r} - \mathbf{r}') \delta(t - t') \delta_{\alpha\beta}. \quad (2.3)$$

An overbar denotes an average with respect to the thermodynamic equilibrium ensemble with temperature T .

In natural conditions turbulence arises either due to the instability of laminar flows (like in channel flow) or due to time dependent stirring (such as in a glass of water stirred by a spoon). For the sake of theoretical simplicity we will model all these situations with a stirring force $\phi(\mathbf{r}, t)$. The properties of the turbulent flow may depend on the nature of the stirring force $\phi(\mathbf{r}, t)$. Since in experimental situations one finds that the statistics of the turbulent velocity field on the large scales are close to that of a Gaussian random ensemble, it is customary to take $\mathbf{f}(\mathbf{r}, t)$ to be a Gaussian random force with spectral support in the small wave vectors and small frequencies. The properties of the correlation function of $\phi(\mathbf{r}, t)$ are best stated in \mathbf{k}, ω space: it is concentrated in the small k, ω region, i.e. $k \leq 1/L$, $\omega \leq U_L$ where U_L is the characteristic magnitude of turbulent velocity fluctuations. In order to model properly the generic properties of turbulent fluids one needs to assume that the correlation decays sufficiently quickly to zero for $k \gg 1/L$, $\omega \gg U_L/L$. In \mathbf{r}, t space it means that $D(R, \tau)$,

$$D_{\alpha\beta}(R, \tau) = \langle\langle \phi_\alpha(\mathbf{r} + \mathbf{R}, t + \tau) \phi_\beta(\mathbf{r}, t) \rangle\rangle \quad (2.4)$$

is constant for $r \ll L$, $\tau \ll L/U$ and for higher values of R and τ it decays quickly. One of the important questions that the theory should address is whether the properties of turbulence on scales much smaller than L are independent of the precise choice of $D(R, \tau)$. Also, the possible effect of non-Gaussianity of the forcing should be understood.

Adding the stirring force to the equation of motion we write

$$\partial \mathbf{u} / \partial t + (\mathbf{u} \cdot \nabla) \mathbf{u} - \nu \nabla^2 \mathbf{u} - \nabla p = \mathbf{f} + \boldsymbol{\phi} . \quad (2.5)$$

The combination $\mathbf{f} + \boldsymbol{\phi}$ will be referred to, when convenient, as $\tilde{\mathbf{f}}$.

In this work we deal with incompressible turbulence only, in which $\nabla \cdot \mathbf{u} = 0$. We shall therefore project out from Eq. (2.5) any longitudinal components. This is done with the help of the projection operator $\overset{\leftrightarrow}{\mathbf{P}}$ which is formally written as $\overset{\leftrightarrow}{\mathbf{P}} \equiv -\nabla^{-2} \nabla \times \nabla \times$. In tensor notation this operator is $P_{\alpha\beta} = \delta_{\alpha\beta} - \nabla^{-2} \nabla_\alpha \nabla_\beta$. Because of the inverse Laplace operator which is nonlocal in space, the application of $\overset{\leftrightarrow}{\mathbf{P}}$ to any given vector field $\mathbf{a}(\mathbf{r})$ is non local:

$$[\overset{\leftrightarrow}{\mathbf{P}} \mathbf{a}(\mathbf{r})]_\alpha = \int d\mathbf{r}' P_{\alpha\beta}(\mathbf{r} - \mathbf{r}') a_\beta(\mathbf{r}') , \quad (2.6)$$

where $P_{\alpha\beta}(\mathbf{r} - \mathbf{r}')$ is the inverse Fourier transform of $P_{\alpha\beta}(\mathbf{k})$

$$P_{\alpha\beta}(\mathbf{r} - \mathbf{r}') = \int \frac{d\mathbf{k}}{(2\pi)^3} \exp[-i(\mathbf{r} - \mathbf{r}') \cdot \mathbf{k}] P_{\alpha\beta}(\mathbf{k}) . \quad (2.7)$$

The tensor $P_{\alpha\beta}(\mathbf{k})$ in k -representation is

$$P_{\alpha\beta}(\mathbf{k}) = \delta_{\alpha\beta} - \frac{1}{k^2} k_\alpha k_\beta \quad (2.8)$$

and in r -representation

$$P_{\alpha\beta}(\mathbf{r} - \mathbf{r}') = \frac{\delta_{\alpha\beta}}{|\mathbf{r} - \mathbf{r}'|^3} - 3 \frac{(r_\alpha - r'_\alpha)(r_\beta - r'_\beta)}{|\mathbf{r} - \mathbf{r}'|^5} . \quad (2.9)$$

The operator $\overset{\leftrightarrow}{\mathbf{P}}$ has the following properties: (i) $\nabla \cdot \overset{\leftrightarrow}{\mathbf{P}} = \overset{\leftrightarrow}{\mathbf{P}} \cdot \nabla = 0$. (ii) For any divergence-free vector \mathbf{b} , $\overset{\leftrightarrow}{\mathbf{P}} \mathbf{b} = \mathbf{b}$. Applying $\overset{\leftrightarrow}{\mathbf{P}}$ to Eq. (2.5) we find

$$(\partial / \partial t - \nu \nabla^2) \mathbf{u} + \overset{\leftrightarrow}{\mathbf{P}} (\mathbf{u} \cdot \nabla) \mathbf{u} = \overset{\leftrightarrow}{\mathbf{P}} \tilde{\mathbf{f}} . \quad (2.10)$$

Introduce the bare Green's operator \mathbf{G}_0 via the relationship

$$\overset{\leftrightarrow}{\mathbf{G}}_0 \equiv \frac{i}{\partial / \partial t - \nu \nabla^2} \overset{\leftrightarrow}{\mathbf{P}} . \quad (2.11)$$

Using $\overset{\leftrightarrow}{\mathbf{G}}_0$ we can rewrite Eq. (2.10) in the form:

$$\mathbf{u}(\mathbf{r}, t) = \mathbf{u}_0(\mathbf{r}, t) - i\overset{\leftrightarrow}{\mathbf{G}}_0(\mathbf{u} \cdot \nabla)\mathbf{u} , \quad (2.12)$$

where

$$\mathbf{u}_0(\mathbf{r}, t) \equiv -i\overset{\leftrightarrow}{\mathbf{G}}_0\tilde{\mathbf{f}} . \quad (2.13)$$

The meaning of the application of $\overset{\leftrightarrow}{\mathbf{G}}_0$ to any vector field $\mathbf{c}(\mathbf{r}, t)$ is understood by

$$\begin{aligned} \overset{\leftrightarrow}{\mathbf{G}}_0\mathbf{c}(\mathbf{r}, t) &= G_{\alpha\beta}^0(\mathbf{r} - \mathbf{r}', t - t') * \mathbf{c}(\mathbf{r}', t) \\ &\equiv \int d\mathbf{r}' dt' G_{\alpha\beta}^0(\mathbf{r} - \mathbf{r}', t - t') c_\beta(\mathbf{r}', t') , \end{aligned} \quad (2.14)$$

where the kernel $G_{\alpha\beta}^0(\mathbf{r} - \mathbf{r}', t - t')$ is the Green's function of the linear part of Eq. (2.10), and we have introduced the $*$ operation according to the RHS of Eq. (2.14). The explicit representation of $G_{\alpha\beta}^0(\mathbf{r} - \mathbf{r}', t - t')$ is given as the inverse transform in \mathbf{k} and ω

$$\begin{aligned} &G_{\alpha\beta}^0(\mathbf{r} - \mathbf{r}', t - t') \\ &= \int \frac{d\mathbf{k}d\omega}{(2\pi)^4} \exp i[\mathbf{k} \cdot (\mathbf{r} - \mathbf{r}') + \omega(t - t')] G_{\alpha\beta}^0(\mathbf{k}, \omega) . \end{aligned} \quad (2.15)$$

The function $G_{\alpha\beta}^0(\mathbf{k}, \omega)$ is

$$G_{\alpha\beta}^0(\mathbf{k}, \omega) = \frac{P_{\alpha\beta}(\mathbf{k})}{\omega + i\nu k^2} . \quad (2.16)$$

The convention chosen is that $G_{\alpha\beta}^0(\mathbf{k}, \omega)$ is analytic in the upper half of the plane of complex ω . Correspondingly $G_{\alpha\beta}^0(\mathbf{r} - \mathbf{r}', t - t')$ is zero for $t' < t$. This property is known as causality, and it stems from the physical constraint that a response cannot come before its cause. It is obvious that the solution (2.12) involves integrals over all space in \mathbf{r}, t representation because of the inverse operators in $\overset{\leftrightarrow}{\mathbf{G}}_0$ which is a factor function in \mathbf{k}, ω space. The solution involves integrals also in \mathbf{k}, ω space due to the nonlinear term which is a local operator in \mathbf{r}, t space. Thus there is no formal advantage to either representation, and we shall write Eq. (2.12) in the representation invariant form

$$\mathbf{u} = \mathbf{u}_0 + \frac{1}{2}\overset{\leftrightarrow}{\mathbf{G}}^0 * \Gamma_{\mathbf{u}}^{\mathbf{u}} . \quad (2.17)$$

The $*$ and the \cdot operations depend on the representation. In \mathbf{r}, t representation the $*$ operation was defined by Eq. (2.14), and $\Gamma_{\mathbf{u}}^{\mathbf{u}}$ means $2(\mathbf{u} \cdot \nabla)\mathbf{u}$. For later applications we need to consider the operation $\Gamma_{\mathbf{u}}^{\mathbf{u}}$ in which different fields \mathbf{u} and $\tilde{\mathbf{u}}$ are involved. We will interpret $\Gamma_{\mathbf{u}}^{\mathbf{u}}$ in a symmetric fashion, i.e.

$$\Gamma_{\mathbf{u}}^{\mathbf{u}} = -i[(\mathbf{u} \cdot \nabla)\tilde{\mathbf{u}} + (\tilde{\mathbf{u}} \cdot \nabla)\mathbf{u}] . \quad (2.18)$$

In Fourier representation we write

$$\mathbf{u}(\mathbf{k}, \omega) \equiv \int d\mathbf{r} dt \exp[-i(\mathbf{r} \cdot \mathbf{k} + \omega t)] \mathbf{u}(\mathbf{r}, t), \quad (2.19)$$

$$[\mathbf{G}^0 * \mathbf{c}]_{\alpha} = G_{\alpha\beta}^0(\mathbf{k}, \omega) c_{\beta}(\mathbf{k}, \omega), \quad (2.20)$$

and

$$\begin{aligned} [\Gamma_{\cdot\tilde{\mathbf{u}}}]_{\alpha}(\mathbf{k}, \omega) &= \int \frac{d\mathbf{k}'}{(2\pi)^3} \frac{d\mathbf{k}''}{(2\pi)^3} \frac{d\omega'}{2\pi} \frac{d\omega''}{2\pi} \\ &\times \Gamma_{\alpha\beta\gamma}(q, q', q'') u_{\beta}^*(\mathbf{k}', \omega') \tilde{u}_{\gamma}^*(\mathbf{k}'', \omega'') \end{aligned} \quad (2.21)$$

where

$$\begin{aligned} \Gamma_{\alpha\beta\gamma}(q, q', q'') &= (2\pi)^4 (k_{\beta} \delta_{\alpha\gamma} + k_{\gamma} \delta_{\alpha\beta}) \\ &\times \delta(\mathbf{k} + \mathbf{k}' + \mathbf{k}'') \delta(\omega + \omega' + \omega''). \end{aligned} \quad (2.22)$$

In these equations and below we introduced the four dimensional vector $q \equiv \{\mathbf{k}, \omega\}$. The symmetry of (2.21) with respect to exchanging \mathbf{u} and $\tilde{\mathbf{u}}$ is inherited from (2.22).

B. Naive Perturbation Theory for the velocity field

It is natural to seek solutions of Eq. (2.17) in the form

$$\mathbf{u}(\mathbf{r}, t) = \sum_{n=0}^{\infty} \mathbf{u}_n, \quad \mathbf{u}_n \propto \Gamma^n. \quad (2.23)$$

Substituting this in the Navier-Stokes equation in the form (2.17), and collecting terms with the same power in Γ we have a set of recurrence relations starting with

$$\mathbf{u}_1 = \frac{1}{2} \mathbf{G}^0 * \Gamma_{\cdot\mathbf{u}_0}, \quad (2.24)$$

$$\mathbf{u}_2 = \frac{1}{2} \mathbf{G}^0 * \Gamma_{\cdot\mathbf{u}_0}^{\mathbf{u}_1} + \frac{1}{2} \mathbf{G}^0 * \Gamma_{\cdot\mathbf{u}_1}^{\mathbf{u}_0} = \mathbf{G}^0 * \Gamma_{\cdot\mathbf{u}_0}^{\mathbf{u}_1}. \quad (2.25)$$

The last equality follows from the symmetry of Γ which was discussed in the previous section. In fact, we are making full use here of the fact that we study a classical system. In the corresponding quantum mechanical theory the two terms in Eq. (2.25) are distinct due to the non-commutativity of \mathbf{u}_1 and \mathbf{u}_0 which become operators.

The next orders have the form

$$\mathbf{u}_3 = \mathbf{G}^0 * \Gamma_{\cdot\mathbf{u}_0}^{\mathbf{u}_2} + \frac{1}{2} \mathbf{G}^0 * \Gamma_{\cdot\mathbf{u}_1}^{\mathbf{u}_1}, \quad (2.26)$$

$$\mathbf{u}_4 = \mathbf{G}^0 * \Gamma_{\cdot\mathbf{u}_0}^{\mathbf{u}_3} + \mathbf{G}^0 * \Gamma_{\cdot\mathbf{u}_1}^{\mathbf{u}_2}, \quad (2.27)$$

etc. In general,

$$\mathbf{u}_n = \sum_{m=0}^{n/2-1} \mathbf{G}^0 * \Gamma_{\cdot \mathbf{u}_m}^{\cdot \mathbf{u}_{n-m+1}} \quad (n \text{ even}), \quad (2.28)$$

$$\begin{aligned} \mathbf{u}_n = & \sum_{m=0}^{(n-3)/2} \mathbf{G}^0 * \Gamma_{\cdot \mathbf{u}_m}^{\cdot \mathbf{u}_{n-m+1}} \\ & + \frac{1}{2} \mathbf{G}^0 * \Gamma_{\cdot \mathbf{u}_{(n-1)/2}}^{\cdot \mathbf{u}_{(n-1)/2}} \quad (n \text{ odd}). \end{aligned} \quad (2.29)$$

At this point one may substitute lower order \mathbf{u}_m in (2.28) and (2.29) to achieve eventually a solution in terms of \mathbf{u}_0 and \mathbf{G}^0 . For example \mathbf{u}_2 can be written as

$$\mathbf{u}_2 = \mathbf{G}^0 * \Gamma_{\cdot \mathbf{u}_0}^{\cdot (1/2) \Gamma_{\cdot \mathbf{u}_0}^{\cdot \mathbf{u}_0}} \quad (2.30)$$

FIGURES

$$\begin{aligned}
 U &\sim \text{short wavy line} , & u_0 &\sim \text{thin wavy line} , \\
 * \Gamma &: \sim \text{fat dot with three tails} \\
 F &\sim \text{bold wavy line} , & F_0 &\sim \text{thin wavy line} , \\
 G &\sim \text{bold wavy line followed by a straight line} , & G_0 &\sim \text{thin wavy line followed by a straight line} .
 \end{aligned}$$

FIG. 1. Graphical notation for the perturbation expansion. The symbols used are the following: short wavy lines stand for the fluid velocity (think about waves). A thin wavy line stands for \mathbf{u}_0 , whereas a bold wavy line represents the full solution $\mathbf{u}(\mathbf{r}, t)$. A straight line stands for the field $\mathbf{p}(\mathbf{r}, t)$ that is only introduced in Chapter III. The Green's function, which is the response in the velocity to some force is made of a short wavy line and a short straight line representing the force. Again this symbol appears in thin and bold variants. The former stands for the bare Green's function (2.11), and the bold for the dressed Green's function (3.5). The vertex (2.18) is a fat dot with three tails. One straight tail belongs to the Green's function, and two wavy tails stand for velocities. A long wavy line will represent correlation functions of velocities. Again, the thin and bold variants are bare and dressed correlators respectively.

For higher values of n this substitution becomes increasingly more cumbersome in analytic form, and it is very helpful to represent it graphically. The notation used is shown in Fig. 1. In Fig. 2a we display the diagrammatic representation of the equation of motion, and in Fig. 2b and Fig. 2c we show the diagrammatic form of Eqs. (2.24) and (2.30). Examining the other graphs in Fig. 2 we see the great advantage of the diagrammatic representation. It is very easy to write the n 'th order diagrams without going through the cumbersome analytic substitutions. The rules for drawing the diagrams are very simple: for the n 'th order term we draw all the topologically distinct binary trees with n vertices, such that all the trunks are made of Green's functions and all the end branches are made of \mathbf{u}_0 's. Every portion of the tree that continues in a symmetric fashion gets a factor of $1/2$. That is all. The existence of these simple rules for finding the n 'th order term, which are independent of n , reflects the internal structure of this perturbation theory, and it will allow us to perform resummations in a straightforward way.

It should be understood that the perturbation theory described in this section is not expected to converge. Consider for example the ratio of \mathbf{u}_1 over \mathbf{u}_0 . "Dividing" Eq. (2.24)

by u_0 leaves us with the order of magnitude estimate

$$\mathbf{u}_1/\mathbf{u}_0 \sim \mathbf{G}^0 * \Gamma \cdot \mathbf{u}_0 \sim \nabla \mathbf{u}_0 / \nu \nabla^2 \sim \mathbf{u}_0 L / \nu = \text{Re} . \quad (2.31)$$

We see that we are effectively expanding in Reynolds number, and for high Re this is a terribly divergent series. The main problem in this expansion is the appearance of the molecular viscosity ν in the denominator in (2.31). It is expected that in a turbulent fluid the viscosity is strongly renormalized because of the interaction, yielding the so called “eddy-viscosity”. We need to reformulate the theory such that the eddy-viscosity appears in the effective expansion parameter to make it of order 1. This is achieved in Sect.2.

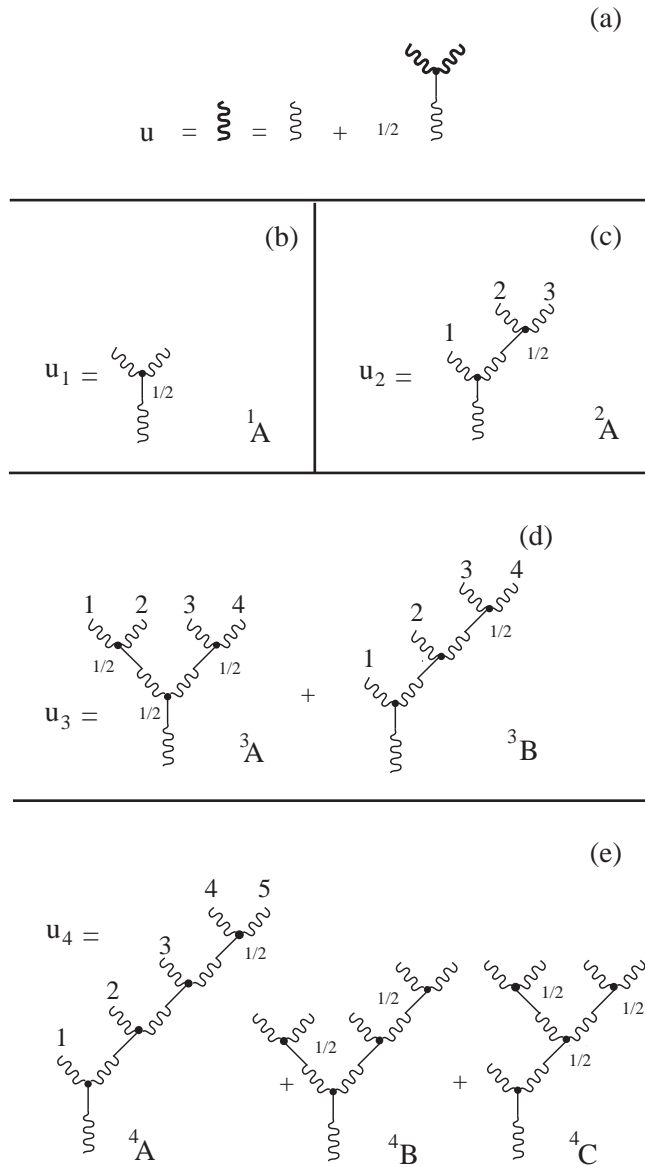


FIG. 2. Graphic representation of the equation of motion [Panel (a)] and the naive perturbation theory. The diagrams in Panels (b)-(d) are all the contributions appearing in $\mathbf{u}_1 - \mathbf{u}_4$. Note that all the topologically distinct trees appear. These trees have a trunk that begins with the wavy line of a bare Green's function, and continues all the way via bare Green's functions. The branches are made of wavy lines of \mathbf{u}_0 . The bifurcations carry a vertex Γ . The factors of $1/2$ appear in all the bifurcations that have symmetry above them. The total factor in front of a tree is the product of these numbers. Every tree has been denoted with a letter and a superscript. The latter stands for the order in Γ^n . For future purposes we have numbered the branches of the trees ${}^2A, {}^3A, {}^3B$ and 4A .

C. Naive perturbation theory for statistical quantities

1. Statistics

As explained in the Introduction, our aim is to formulate a theory for ergodic averages. In the naive perturbation theory we can compute such averages by using the expansion (2.23) for $\mathbf{u}(\mathbf{r}, t)$, and averaging products of $\mathbf{u}_0(\mathbf{r}, t)$ at different points and times with respect to different realizations of the random forcing $\tilde{\mathbf{f}}$. In doing so we shall make full use of the fact that $\tilde{\mathbf{f}}$ is assumed to be Gaussian. On the one hand, this leads to a great simplification of the naive perturbation theory. On the other hand it seems theoretically dangerous. The physics that we are trying to describe is surely non-Gaussian. Are we not throwing away important aspects of the physics by using from the start a Gaussian forcing? The answer will be NO. We shall see later that the structure of the theory in its final resummed formulation does not depend on this way of constructing the naive expansion. The physics is dominated by strong interactions via the nonlinearity, and a Gaussian forcing is sufficient to excite all the possible responses which the dynamics amplifies and redistributes to allow us to observe the full statistical structure. In fact, at the end of the calculation we are going to explore the limit in which the random forcing becomes vanishingly small. We shall show that this limit exists, and that in that limit the statistics of velocity fluctuations becomes independent of the statistics of the random force. Notwithstanding, it should be said here that it is not at all obvious that the procedure followed here is the most *efficient* one. It is possible that one can get a better converging theory by forcing the system with a force that is closer in

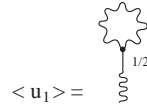
character to the statistics of the dressed system. We do not know how to do that, and this is one of the open problems that needs to be studied in the future. We shall return to this issue in Sec. 3 after the formal apparatus needed for its full appreciation is already at hand.

We will denote averages with respect to the realization of the random force with single pointed brackets, in contrast with the double pointed brackets of Eq. (1.1). The Gaussianity of the random force means that

$$\begin{aligned}
 \langle \tilde{\mathbf{f}}(x) \rangle &= 0, \\
 \langle \tilde{\mathbf{f}}(x_1) \tilde{\mathbf{f}}(x_2) \rangle &= D_{12}, \\
 \langle \tilde{\mathbf{f}}(x_1) \tilde{\mathbf{f}}(x_2) \tilde{\mathbf{f}}(x_3) \rangle &= 0 \\
 \langle \tilde{\mathbf{f}}(x_1) \tilde{\mathbf{f}}(x_2) \tilde{\mathbf{f}}(x_3) \tilde{\mathbf{f}}(x_4) \rangle &= D_{12}D_{34} + D_{13}D_{24} + D_{13}D_{23},
 \end{aligned}
 \tag{2.32}$$

etc. All higher order correlations with odd number $\tilde{\mathbf{f}}$ vanish, and the correlations involving $2n$ factors of $\tilde{\mathbf{f}}$ have $(2n - 1)!!$ contributions corresponding to all the possible pairings of $\tilde{\mathbf{f}}$.

(a)



(b)

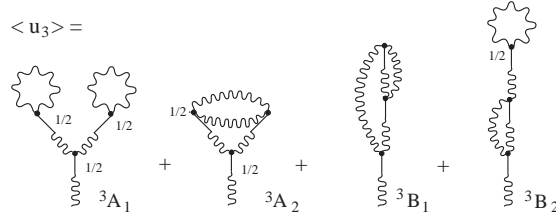


FIG. 3. The diagrams representing the mean velocity. Panel (a) represents the first order contribution in Γ , and is obtained from the simple gluing of the two branches of the tree 1A in Fig. 2b. It carries the factor of $1/2$ which originates from the symmetry of 1A . Clearly, averaging either 2A of Fig. 2c or any tree in Fig 2e results in a zero contribution due to the odd number of branches which carry a random force: $\langle \mathbf{u}_2 \rangle = \langle \mathbf{u}_4 \rangle = 0$. Panel (b) represents the result of averaging of the trees 3A and 3B in Fig. 2d. The diagram 3A_1 originates from gluing of the branches 1 with 2 and 3 with 4 in 3A . Diagram 3A_2 comes from gluing either 2 with 3 and 1 with 4 or 1 with 3 and 2 with 4 in 3A . Correspondingly we gain a factor of 2 with 3A_2 leading to a coefficient $1/4$ instead of $1/8$ in 3A . The tree 3B_1 originates from 3B after gluing 1 with 3 and 2 with 4 or 1 with 4 and 2 with 3. A factor of 2 is gained. Lastly, diagram 3B_2 results from gluing 1 with 2 and 3 with 4 in 3B . There is only one way of doing it, and the factor $1/2$ remains. The general rule for the overall factor in front of a diagram is obtained as follows: count the number of vertices such that that exchanging the two branches emanating from them leaves the diagram invariant. Denote the number of distinct pairs of such branches by N . The overall factor in front of the diagram is $1/2^N$.

2. The mean velocity

Of the sought statistical quantities, the easiest to obtain is the mean velocity, averaged over all the possible realizations of the random force. Since this random force is Gaussian, we have well defined statistics for the averaging process. We can apply the rules (2.32) to the average of the diagrammatic representation of $\mathbf{u}(\mathbf{r}, t)$. We pair the \mathbf{u}_0 branches in all the possible ways, and glue the ends together, see Fig. 3. Every diagram with an odd number of \mathbf{u}_0 branches gives no contribution. Every diagram with $2n$ \mathbf{u}_0 branches gives $(2n-1)!!$ contributions which are obtained from all the possible binary pairings of random forces. The process is shown in Fig. 3. The diagrams nA_m and nB_m for $\langle \mathbf{u}_n \rangle$ in Fig. 3 result from the diagrams nA and nB for \mathbf{u}_n in Fig. 2. Note that in systems which are homogeneous and isotropic the mean velocity vanishes. Consequently, the sum of all the diagrams obtained in this fashion has to vanish. This will be used in our later developments. In a turbulent system with a space dependent mean velocity profile this set of diagrams will not vanish, and it will contribute also in other statistical averages that we consider below. These diagrams will describe the interaction of the mean profile with the velocity fluctuations.

3. The Green's function

Next we discuss the Green's function, which is the response of the velocity field to an external perturbation. The Green's function is defined as

$$G_{\alpha\beta}(x, x') = i \langle \delta u_\alpha(x) / \delta \tilde{f}_\beta(x') \rangle \quad (2.33)$$

where the notation $\delta(\cdot)/\delta(\cdot)$ stands for the functional derivative. The meaning of this functional derivative is the following: solve the Navier-Stokes equations once with a forcing $\tilde{\mathbf{f}}$ and once with a forcing $\tilde{\mathbf{f}} + \epsilon\delta(x - x')$. Then take the ratio $[\mathbf{u}(x, \epsilon) - \mathbf{u}(x, 0)]/\epsilon$ in the limit $\epsilon \rightarrow 0$, and average over the realizations of the random force. The principle of causality means that $\mathbf{G}(x, x')$ is zero for $t' < t$. This property will be used a lot in the sequel.

The calculation of the functional derivative using the diagrams in Fig. 2 is straightforward. Every diagram having n branches of \mathbf{u}_0 contains a product of n $\tilde{\mathbf{f}}$'s. The calculation of the derivative with respect to $\delta\tilde{\mathbf{f}}(x')$ means via the chain rule that we get n contributions to $\delta\mathbf{u}(x)/\delta\tilde{\mathbf{f}}(x')$. Every such contribution is obtained by dropping one of the branches of \mathbf{u}_0 , and replacing it by branch of \mathbf{G}^0 . An example of how this procedure is done for diagrams 2A and 4A in Fig. 2 is shown in Fig. 4a and Fig. 4b respectively.

The second step is obtained by averaging the diagrams for $\delta\mathbf{u}(x)/\delta\tilde{\mathbf{f}}(x')$ over realizations of $\mathbf{f}(x')$. We can apply the rules (2.32) to the averages of the diagram of $\delta\mathbf{u}(x)/\delta\tilde{\mathbf{f}}(x')$ in a graphical sense. This procedure is done in Fig. 5. Fig. 5a contains the two contributions to \mathbf{G}_2 , and Figs. 5b and 5c show all the 19 diagrams for \mathbf{G}_4 . The diagram denoted ${}^nA_{mp}$ are obtained from the diagrams nA_m in Fig. 4. The diagrams denoted ${}^nB_{mp}$ and ${}^nC_{mp}$ originate from diagrams nB and nC in Fig. 2. Notice that every diagram has an "entry" which is the root of the tree in Fig. 2, and an "exit" which is the branch \mathbf{G}^0 which replaced a branch of \mathbf{u}_0 . There is a unique path between entry and exit which is composed of a chain of \mathbf{G}^0 's. We shall call this path the "principal path" of the diagram. Notice that the entry always begins with a wavy line, whereas the exit ends with a straight line. In fact, all the diagrams appearing here can be drawn without reference to the explicit derivation described here using simple topological rules. However, since the diagrams described here are not in their final form we defer the discussion of the appropriate rules for a later moment.

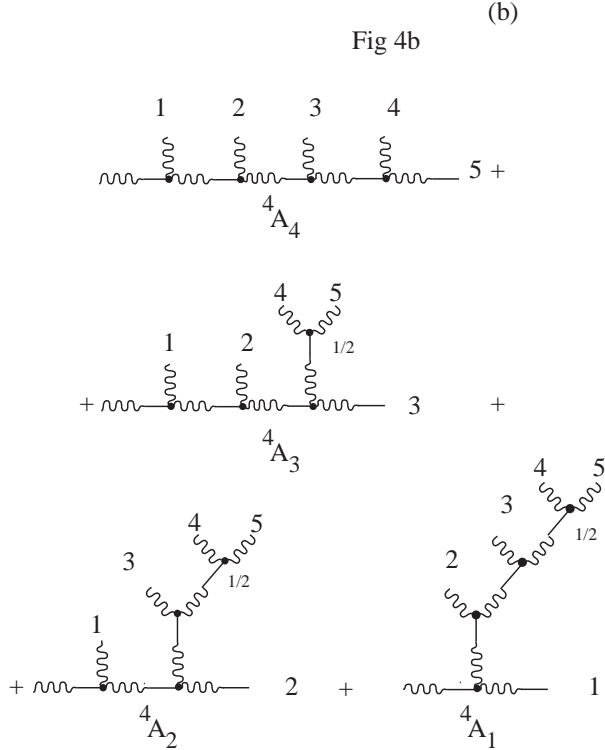
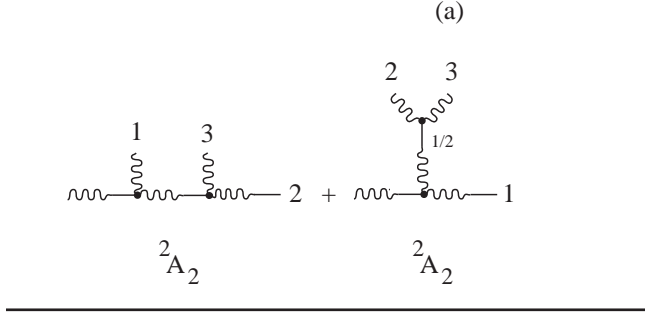


FIG. 4. Typical contribution to the diagrammatic representation of $\delta \mathbf{u}(x)/\delta \tilde{\mathbf{f}}$ which originates from the trees 2A and 4A in Fig. 2c and 2e. In panel (a) we show the diagrams originating from 2A and in panel (b) those originating from 4A . The diagram 2A_2 is obtained by differentiating with respect to $\tilde{\mathbf{f}}(x')$ at position 2 or 3 in 2A . A factor of 2 is gained. The diagram 2A_1 comes from differentiating with respect to $\tilde{\mathbf{f}}(x')$ at position 1. The diagram 4A_4 is obtained by differentiating with respect to $\tilde{\mathbf{f}}(x')$ at position 4 or 5 in 4A . A factor of 2 is gained. The diagrams 4A_3 , 4A_2 and 4A_1 come from differentiating with respect to $\tilde{\mathbf{f}}(x')$ at positions 3, 2 and 1 respectively. Again the factor 1/2 remains at vertices that have symmetry above them.

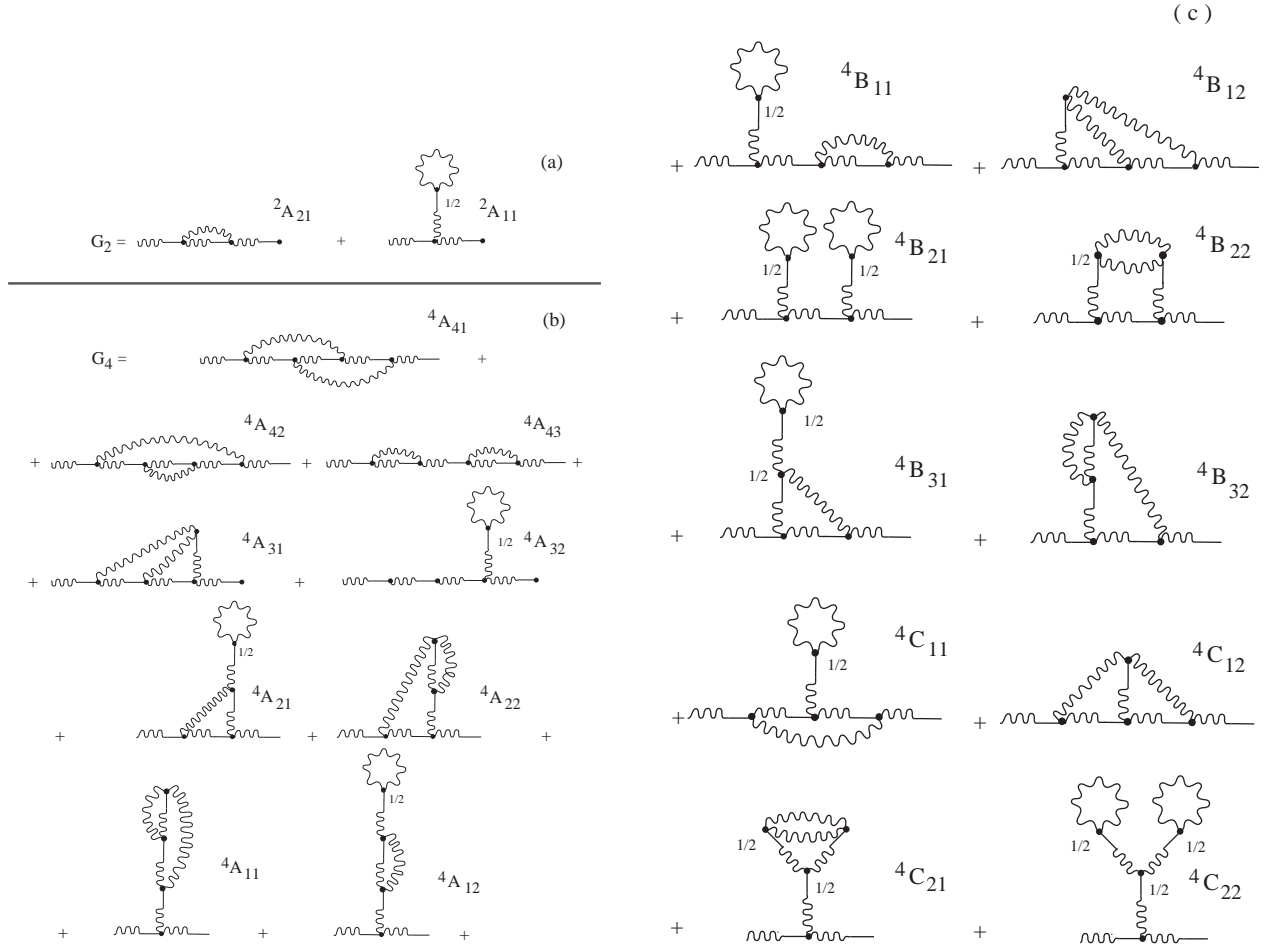


FIG. 5. Diagrams for the Green's function. Panel (a): The contributions to \mathbf{G}_2 originate from the trees shown in Fig. 4a by gluing two \mathbf{u}_0 branches in the only possible way. Panel (b): The contributions to \mathbf{G}_4 originating from the trees ${}^4A_1 - {}^4A_4$ shown in Fig. 4b. The diagrams ${}^4A_{41} - {}^4A_{43}$ come from 4A_4 by gluing 1 - 3 and 2 - 4; 1 - 4 and 2 - 3 ; 1 - 2 and 3 - 4 respectively. The diagrams ${}^4A_{31}$ come from 4A_3 by gluing 1 - 4 and 2 - 5 *or* 1 - 5 and 2 - 4. A factor of 2 is gained. ${}^4A_{32}$ is obtained by gluing 4A_3 at positions 1 - 2 and 4 - 5. The diagram ${}^4A_{21}$ comes from 4A_2 by gluing 1-3 and 4-5. ${}^4A_{22}$ is obtained by gluing 1-4 and 3-5 *or* 1-5 and 3-4, gaining a factor of 2. Finally ${}^4A_{11}$ comes from 4A_1 by gluing 2-4 and 3-5 *or* 2-5 and 3-4. ${}^4A_{12}$ obtains from 4A_1 by gluing 2-3 and 4-5. (c) Diagrams for \mathbf{G}_4 originating from 4B and 4C in Fig. 2e. Note that again all the numerical factors follow the same rules as observed in Fig. 4.

4. The 2-point velocity correlation function

The 2-point velocity correlation function $\mathbf{F}(x, x')$ is defined as

$$F_{\alpha\beta}(x, x') = \langle u_\alpha(x)u_\beta(x') \rangle . \quad (2.34)$$

The calculation of this quantity is again based on the diagrammatic expansion shown in Fig. 2. To obtain \mathbf{F}_{m+p} of order Γ^{m+p} we need first to take a contribution \mathbf{u}_m and a contribution \mathbf{u}_p and multiply them together. The n -th order \mathbf{F}_n is obtained as a sum of all \mathbf{F}_{m+p} such that $m + p = n$. In the second step we average over the realizations of $\tilde{\mathbf{f}}$. As before all odd order contributions vanish because they contain an odd power of $\tilde{\mathbf{f}}$. For example,

$$\begin{aligned} \mathbf{F}_0(x, x') &= \mathbf{F}_{0+0}(x, x'), \\ \mathbf{F}_1(x, x') &= \mathbf{F}_{1+0}(x, x') + \mathbf{F}_{0+1}(x, x') = 0, \\ \mathbf{F}_2(x, x') &= \mathbf{F}_{2+0}(x, x') + \mathbf{F}_{1+1}(x, x') + \mathbf{F}_{0+2}(x, x'), \end{aligned} \quad (2.35)$$

where

$$\mathbf{F}_{m+p}(x, x') = \langle \mathbf{u}_m(x)\mathbf{u}_p(x') \rangle . \quad (2.36)$$

To obtain the diagrammatic representation of this procedure we take one tree for $\mathbf{u}_m(x)$ and one tree for $\mathbf{u}_p(x')$ from Fig. 2, and average the product of these trees according to the rules (2.32). In other words we need to pair the branches of \mathbf{u}_0 in all the possible ways, and to glue them as discussed before in computing $\langle \mathbf{u} \rangle$ and the Green's function. The procedure is shown in Fig. 6. Note that every diagram has a uniquely defined "principal cross section" which arises from the gluing of the two trees $\mathbf{u}_m(x)$ and $\mathbf{u}_p(x)$. We denote it in the diagrams as a vertical broken line, and we draw the reader's attention to the fact that the principal cross section cuts through correlators only, and not through Green's functions. This fact is used later in the process of resummation.

This is the end of the naive perturbation theory. As we saw, it is an expansion in powers of Re , and we are going to partly resum this expansion to develop a reformulation with a better expansion parameter. We reiterate here that the procedure at this point seems very dependent on the properties of the noise, since we used the rules (2.32) time and again. We defer further discussion of this issue until after the resummations of various sorts, when we can take the limit $\tilde{\mathbf{f}} \rightarrow 0$ with impunity.

3. RESUMMATIONS

In this chapter we discuss the resummation of the naive perturbation theory that was developed in Chapter 2. We begin with the mean velocity and its role in the resummation of the Green's function and the correlator.

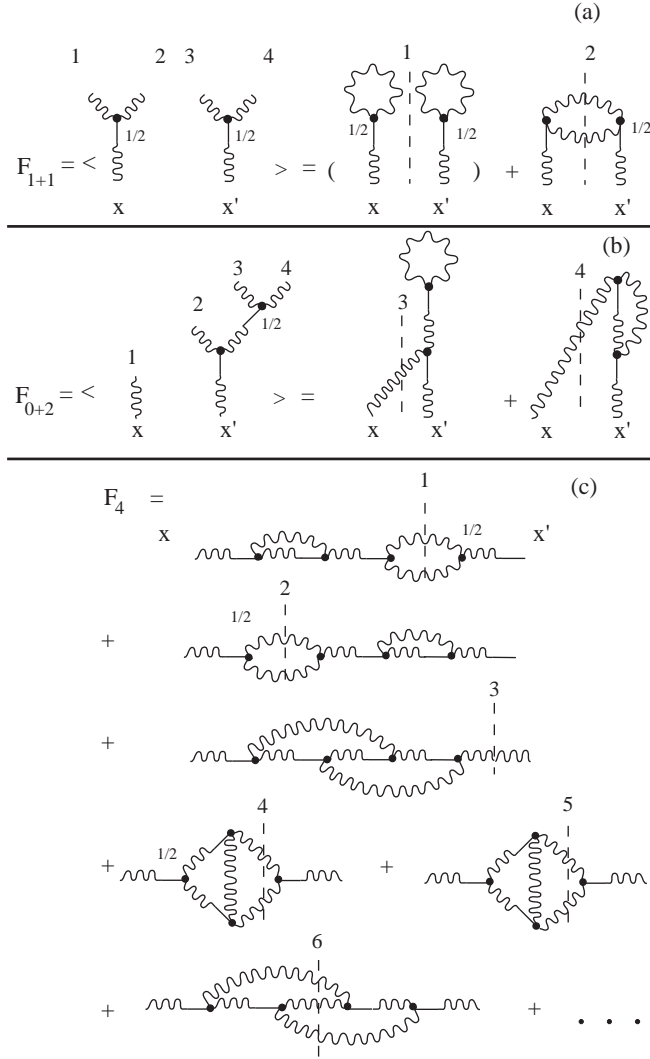


FIG. 6. Diagrammatic representation of the 2-point velocity correlation function. Panel (a): \mathbf{F}_{1+1} is obtained from the trees $\mathbf{u}_1(x)$ and $\mathbf{u}_1(x')$. Diagram 1 is obtained by gluing 1-2 and 3-4, and diagram 2 by gluing 1-3 and 2-4 *or* 1-4 and 2-3, gaining a factor of 2. Panel (b): F_{0+2} is obtained from the trees for $\mathbf{u}(x)$ and $\mathbf{u}_2(x')$. Diagram 1 is obtained by gluing 1-2 and 3-4, while the diagram 2 comes from gluing 1-3 and 2-4 *or* 1-4 and 2-3, gaining a factor of 2. Panel (c): Some typical diagrams contributing to \mathbf{F}_4 . Note that all the diagrams have a “principal cross section” that separates trunks belonging to the left and to the right trees. This cross section runs through 2-point correlators, never through Green’s functions. In contrast with the diagrams for the Green’s function that have wavy entries and straight exits, here we have wavy entries on both sides. The rules for the numerical factors of the diagrams remain the same.

A. The resummation of the mean velocity

In Section 2B we discussed the diagrammatic series for $\langle \mathbf{u} \rangle$ (see Fig. 3), and commented that it has to sum up to zero when $\langle \mathbf{u} \rangle = 0$. In discussing the diagrams for the Green’s function Fig. 5 and for the correlator Fig. 6 we encounter again the same type of diagrams that appear in $\langle \mathbf{u} \rangle$. For example in Fig. 5 the diagrams ${}^2A_{11}$, ${}^4A_{32}$, ${}^4A_{21}$, ${}^4A_{11}$, ${}^4B_{21}$, ${}^4B_{31}$, and ${}^4C_{11}$ all have a fragment which is the diagram for $\langle \mathbf{u}_1 \rangle$ in Fig. 3a. In addition, the diagram ${}^4A_{11}$ has a fragment which is identical to 3B_1 in Fig. 3. The diagram ${}^4A_{12}$ has a fragment like 3B_2 . The diagram ${}^4C_{21}$ has a fragment like 3A_2 , and lastly ${}^4C_{22}$ exhibits a fragment like 3A_1 .

All these diagrams that contain fragments belonging to $\langle \mathbf{u} \rangle$ have a common feature. To see this denote the part of any diagram that contains the principal path between entry and exit as the “body” of the diagram. Any fragment that can be disconnected from the body by cutting one Green’s function is called a “weakly linked” fragment. All the diagrams that we discussed in the previous paragraph have weakly linked fragments. Consider now all the diagrams in Fig. 5 that have two Green’s functions in their principal path. These are the diagrams ${}^2A_{11}$, ${}^4A_{11}$, ${}^4A_{12}$, ${}^4C_{21}$ and ${}^4C_{22}$. The sum of the weakly linked fragments of these diagrams is exactly $\langle \mathbf{u}_1 \rangle + \langle \mathbf{u}_3 \rangle$ as can be seen in Fig. 3. If we consider all the higher order diagrams for \mathbf{G} which have two Green’s functions in the principal path, we find that their weakly connected fragments furnish all the remaining diagrams in the series for $\langle \mathbf{u} \rangle$. The coefficients in front of all these fragments is the same as the coefficient in the series for $\langle \mathbf{u} \rangle$

since it is determined uniquely by the local topology of the fragment, independently of the position that the fragment occupies in the mother diagram. Accordingly all these diagrams with two Green's functions in the principal path sum up to zero. The same story repeats for all the diagrams that contain a weakly linked fragment. For example the diagram ${}^4A_{21}$ in Fig 5b is the first in the series that exhibits a weakly linked fragment that eventually will be resummed together with diagrams that have the same body, but higher order weakly linked contributions that sum up to zero. The general conclusion is that all the diagrams that have at least one weakly linked fragment sum up to zero and need not be considered further in the resummed theory.

Next we discuss the appearance of $\langle \mathbf{u} \rangle$ in the series for the 2-point correlation function. In this series we find a new type of diagram, like diagram 1 in Fig. 6a. These are unlinked diagrams which are obtained from averaging the left and the right tree separately. Such diagrams contain no correlators that cross the principal cross section. Obviously such diagrams will resum to $\langle \mathbf{u} \rangle^2$ which is zero. In addition we have diagrams with weakly connected fragments. In the context of the diagrams for the 2-point correlator we define the body of the diagram as the part that contains the two entries (the roots of the original trees), which are denoted by “ x ” and “ x' ” in all the diagrams in Fig. 6. A weakly linked fragment is a fragment that can be disconnected from the body of the diagram by cutting off one Green's function. An example of such a diagram is diagram 1 in Fig. 6b. As in the case of the Green's function, the infinite sets of weakly linked fragments with the same body resums to $\langle \mathbf{u} \rangle = 0$. From this point on we therefore discard all the diagrams that have at least one weakly connected fragment.

B. The Dyson resummation for the Green's function

In this section we discuss the Dyson line resummation of the series for the Green's function. To this aim we classify the diagrams into three classes. The first class consists of diagrams with weakly linked fragments which are all discarded. The other two classes are designated as follows:

I. Principal path reducible diagrams. These are diagrams that can be split into two disjoint pieces which contain more than one Green's function, by cutting one bare Green's function that belongs to the principal path. An example of such a diagram is ${}^4A_{43}$ in Fig. 5b. This diagram fall into two parts by cutting $\mathbf{G}_0(x_2, x_3)$.

II. Principal path irreducible diagrams. These are the diagrams that cannot be split as

described in I. All the other diagrams in Fig. 5 that do not have weakly linked fragments are principal path irreducible.

All the principal path irreducible diagrams, except $\mathbf{G}_0(x, x')$ itself, share the property that they start with a bare $\mathbf{G}_0(x, x_1)$, they end up with a bare $\mathbf{G}_0(x_2, x')$, and in between they have a principal path irreducible structure, say $S(x_1, x_2)$. The sum of all these irreducible structures is defined as the Σ operator, which will be shown to contain all the information about the turbulent eddy viscosity. Using the diagrams in Fig. 5 we develop the diagrammatic expansion for $\Sigma(x, x_1)$ which is shown in Fig. 7. With the help of $\Sigma(x_1, x_2)$ we can say that the sum of all the principal path irreducible diagrams is

$$\begin{aligned} & \text{Sum of all irreducibles} & (3.1) \\ & = \mathbf{G}_0(x, x') + \mathbf{G}_0(x, x_1) * \Sigma(x_1, x_2) \cdot \mathbf{G}_0(x_2, x') \end{aligned}$$

where the star “*” and dot “.” products are as defined in the vertex Eq. (2.17). The operator $\Sigma(x_1, x_2)$ starts and ends with a vertex, and it therefore connects with “*” to the preceding $\mathbf{G}_0(x, x_1)$, and with a “.” to the following $\mathbf{G}_0(x_2, x')$. Further summation of this series will be discussed soon.

The principal path reducible diagrams, of which we have only one representative in Fig. 5, can be also resummed using the operator $\Sigma(x_1, x_2)$. Note that the reducible diagram ${}^4A_{43}$ has a structure such that that between x_1 and x_2 there exists the first contribution to $\Sigma(x_1, x_2)$, and after the point x_2 we see a fragment that is identical to ${}^2A_{21}$, which is the first nonlinear contribution to the Green’s function. The main observation, which is due to Dyson, is that higher order reducible diagrams will have between x_1 and x_2 all the higher order terms in $\Sigma(x_1, x_2)$, and than after x_2 we will have all the other nonlinear contributions to the Green’s function $\mathbf{G}(x_2, x')$. Therefore, we can write

$$\begin{aligned} & \text{Sum of all reducibles} & (3.2) \\ & = \mathbf{G}_0(x, x_1) * \Sigma(x_1, x_2) \cdot [\mathbf{G}(x_2, x') - \mathbf{G}_0(x_2, x')] \end{aligned}$$

Again we made use of the fact that all topologically possible diagrams appear in the series, and that the numerical weight of each fragment is only determined by its local symmetry, independent of its position in the mother diagram.

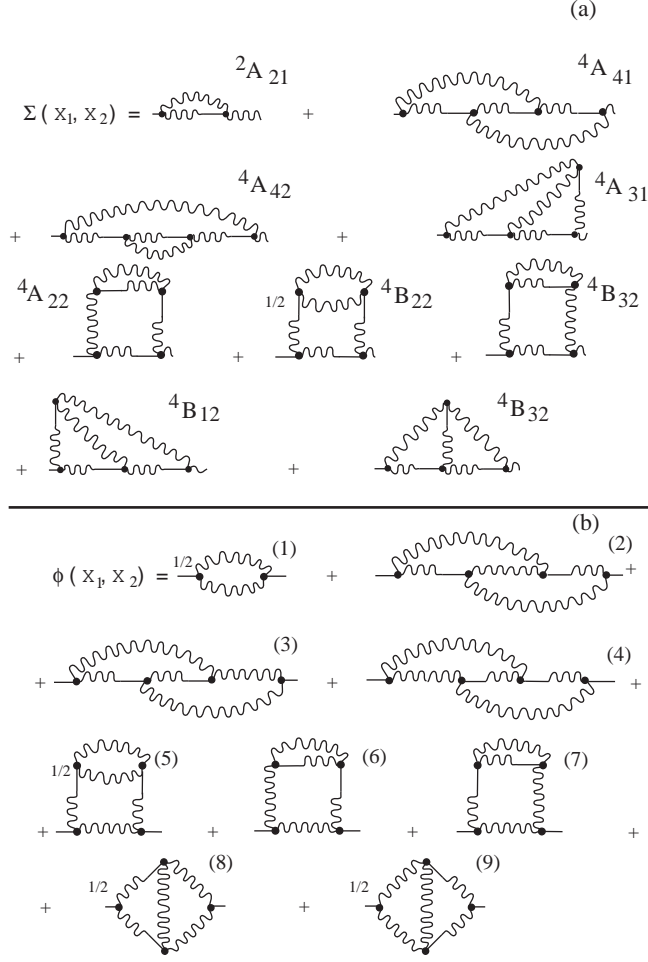


FIG. 7. Panel (a): Diagrammatic series for the $\Sigma(x_1, x_2)$ operator. All the diagrams to order Γ^4 are shown. Every diagram is denoted by the same notation of the diagram it derives from in Fig. 5. Panel (b): Diagrammatic series for the $\Phi(x_1, x_2)$ operator. All the diagrams to order Γ^4 are shown. The numbering of the diagrams is referred to in the section on line resummation.

Adding together (3.1) and (3.2) we get the Dyson equation for the Green's function

$$\mathbf{G}(x, x') = \mathbf{G}_0(x, x') + \mathbf{G}_0(x, x_1) * \Sigma(x_1, x_2) \cdot \mathbf{G}(x_2, x') \quad (3.3)$$

The formal solution of this equation in operator form is

$$\overleftrightarrow{\mathbf{G}} = [\mathbf{1} - \overleftrightarrow{\mathbf{G}}_0 * \overleftrightarrow{\Sigma}]^{-1} \overleftrightarrow{\mathbf{G}}_0 \quad (3.4)$$

or, more explicitly

$$\overleftrightarrow{\mathbf{G}} = [\overleftrightarrow{\mathbf{G}}_0^{-1} - \overleftrightarrow{\Sigma}]^{-1} = \left[\frac{i\overleftrightarrow{\mathbf{P}}}{\partial/\partial t - \nu\nabla^2 - \overleftrightarrow{\mathbf{P}}\overleftrightarrow{\Sigma}} \right] \quad (3.5)$$

where we insert the definition of $\overset{\leftrightarrow}{\mathbf{G}}_0$ from the Eq. 2.11) has been used. We see now that the $\overset{\leftrightarrow}{\Sigma}$ operator serves as a renormalization of the viscosity. The full appreciation of this fact will become clear in subsection D.

C. The Wyld resummation for the 2-point correlation function

In this section we discuss the Wyld line resummation of the series of the 2-point correlation function. We need again to classify the diagrams in order to see clearly how to proceed. Firstly, all the diagrams that are unlinked or have weakly linked fragments can be discarded. Next we consider all the diagrams that have only one wavy line that crosses the principal cross section. The diagram 2 in Fig. 6b and the diagram 3 in Fig. 6c are such diagrams. In Fig. 8 we show a typical 8th order diagram of this type.

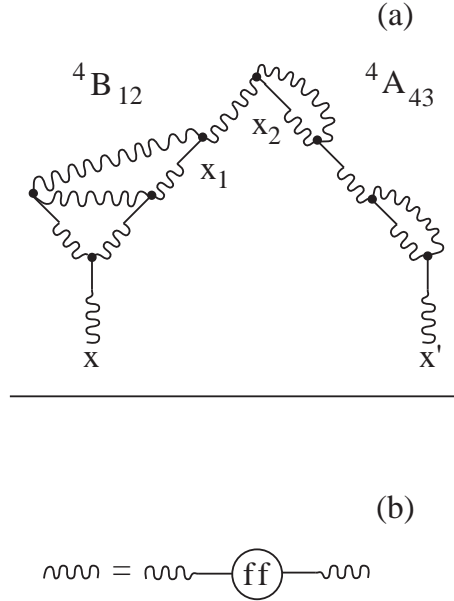


FIG. 8. Panel (a). One of the diagrams that have one wavy line at the principal cross section which appears in the series for the 2-point correlation function. Panel (b). The representation of the lowest order contribution to the 2-point correlator

Recall now that the wavy line, which is a correlation function of two \mathbf{u}_0 's, $\langle \mathbf{u}_0(x) \mathbf{u}_0(x') \rangle$, can be interpreted as $\mathbf{G}_0(x, x_1) * \langle \tilde{\mathbf{f}}(x_1) \tilde{\mathbf{f}}(x_2) \rangle * \mathbf{G}_0(x_2, x')$ (see Fig. 8b). Thus, on the two sides of the $\langle \tilde{\mathbf{f}}(x_1) \tilde{\mathbf{f}}(x_2) \rangle$ we have two typical contributions to the diagrammatic series of \mathbf{G} that was discussed in the last section. On both sides of the principal cross section we get, excluding $\langle \tilde{\mathbf{f}}(x_1) \tilde{\mathbf{f}}(x_2) \rangle$, portions of diagrams that have an entry and an exit like all the

diagrams in Fig. 5. Thus the diagrams 2 in Fig. 6b and 3 in Fig. 6c have fragments which are identical to ${}^2A_{21}$ in Fig. 5a. In the example of Fig. 8 the two fragments are identical with diagrams ${}^4B_{12}$ and ${}^4A_{43}$ in Fig. 5. All the other diagrams with only one wavy line across the principal cross sections will have all the other contributions to the series of \mathbf{G} on both sides of the $\langle \tilde{\mathbf{f}}(x_1)\tilde{\mathbf{f}}(x_2) \rangle$ correlation. Thus we conclude that

$$\begin{aligned} & \text{Sum of all diagrams with one} \\ & \text{wavy line at the cross section} \\ & = \mathbf{G}(x, x_1) * \langle \tilde{\mathbf{f}}(x_1)\tilde{\mathbf{f}}(x_2) \rangle * \mathbf{G}(x_2, x') . \end{aligned} \quad (3.6)$$

Next we consider the diagrams with two or more wavy lines crossing the principal cross section. Examples are diagram 2 in Fig. 6a, and diagrams 1,2,4, 5 and 6 in Fig. 6c. Of these diagrams consider first all those that cannot be split into two parts (containing more than a single Green's function) by cutting off one Green's function. All these diagrams have two entries via straight lines on the right and the left, and a structure, say $\phi(x_1, x_2)$ in between. The sum of all these $\phi(x_1, x_2)$ contributions is defined as the $\Phi(x_1, x_2)$ operator. In Fig. 7b all the contributions of $\Phi(x_1, x_2)$ up to 4th order are exhibited.

All the rest of the diagrams that have two or more wavy lines crossing the principal cross section are analyzed as follows: start from the principal cross section, and move left until you meet for the first time a Green's function that can be cut such that the diagram splits into two disjoint parts. Denote the coordinate of the vertex at the exit of this Green's function as x_1 . Start again from the the principal cross section and move the right until you meet another Green's function that can be cut such that the diagram splits into two parts. Denote the coordinate at the vertex at the exit by x_2 . This notation is shown in all the relevant diagrams of Fig. 6. The fragment to the left of x_1 and to the right of x_2 is a typical fragment that appears in the series for \mathbf{G} . For example in diagram 2 Fig. 6a we have a $\mathbf{G}_0(x, x_1)$ on the left of x_1 and $\mathbf{G}_0(x_2, x')$ on the right of x_2 . In diagram 1 in Fig. 6c we have a fragment ${}^2A_{21}$ (Fig. 5) to the left of x_1 and again \mathbf{G}_0 to right of x_2 . In the diagram 2 in Fig. 6c we have the inverted situation. Obviously, in the higher order diagrams we will find all the remaining contributions to \mathbf{G} . We thus conclude that all these diagrams which have two or more wavy lines crossing the principal cross section may be resummed to

$$\begin{aligned} & \text{Sum of all diagrams with 2 and more} \\ & \text{wavy lines crossing the cross section} \\ & = \mathbf{G}(x, x_1) * \Phi(x_1, x_2) * \mathbf{G}(x_2, x') . \end{aligned} \quad (3.7)$$

Summing up Eqs.(3.6) and (3.7) we recover the Wyld equation

$$\begin{aligned} \mathbf{F}(x, x') & \\ &= \mathbf{G}(x, x_1) * [\langle \tilde{\mathbf{f}}(x_1) \tilde{\mathbf{f}}(x_2) \rangle + \Phi(x_1, x_2)] * \mathbf{G}(x_2, x') . \end{aligned} \tag{3.8}$$

This equation, after the resummation of the series for Φ , will allow us to discuss the limit $\tilde{\mathbf{f}} \rightarrow 0$.

D. Line resummation

Up to now our perturbation series is in orders of the Re number, as explained in Sect.2. The Green's function and the 2-point correlators which appear in the diagrams for Φ and Σ are the bare ones. In this section we perform the so called "line resummation" which results in diagrams in which all the propagators are dressed ones, and at the same time the perturbation parameter becomes of the order of 1.

To accomplish this resummation we introduce a few notions. First is the notion of the "end points" of a diagram. The end points are defined as the entry and exit in the case of the diagrams for Σ , and the two exits in the case of diagrams for Φ . Next we define "one eddy reducible" diagrams and "one-eddy irreducible" diagrams. These types of diagrams play a topologically similar role to the "one-particle reducible and irreducible" diagrams in the standard Feynman diagrams. The definition is as follows: Name as a "one-eddy reducible" fragment any fragment that can be completely disjointed from the part of a diagram that contains the end points by cutting any two lines, be whether Green's functions or correlators. The part that contains the two end points will be called the bulk of the diagram, which may or may not be the same as the body of the diagram as defined in Section 3 A. The convention will be that the fragment contains the two lines that have been cut. In other words, we cut lines near the vertex that belongs to the rest of the diagram. It follows from this convention that one-eddy reducible diagrams are at least of order Γ^2 . Define now

I. One-eddy reducible diagrams: diagrams that contain at least one one-eddy reducible fragment.

II. One-eddy irreducible diagrams: diagrams that contain no one-eddy reducible fragment.

Examples for one-eddy reducible diagrams are diagrams ${}^4A_{42}$, ${}^4A_{22}$, ${}^4B_{22}$ and ${}^4B_{32}$ in Fig. 7a for Σ , and diagrams 5, 6 and 7 in Fig. 7b for Φ . The rest of the diagrams in Fig. 7 are one-eddy irreducible.

We can classify one-eddy reducible fragments into two classes, called as class \mathbf{F} and class \mathbf{G} . Class \mathbf{F} has two wavy ends (like the fragment of ${}^4A_{22}$) and class \mathbf{G} has one wavy and one straight end (like the fragment of ${}^4A_{42}$). An observation of principal significance is that the sum of all the possible fragments of class \mathbf{F} is precisely the nonlinear correction to the 2-point correlator \mathbf{F} , whereas the sum of all the possible fragments of class \mathbf{G} is the nonlinear correction to the Green's function \mathbf{G} . As an example the fragment of ${}^2A_{42}$ is the first nonlinear correction to \mathbf{G} which is ${}^2A_{21}$ in Fig. 5a. The fragments of ${}^4B_{22}$ in the series for Σ , Fig. 7a and the fragment of diagram 5 in the series for Φ , Fig. 7b are the same, and are the nonlinear correction 2 for \mathbf{F} in Fig. 6a. The fragment of the diagram ${}^4A_{22}$ is the diagram 2 in Fig. 6b.

Consider now the irreducible diagram ${}^2A_{21}$ in Fig. 7a. By summing it together with the one-eddy reducible diagrams whose bulk part contains either one bare correlator or one bare Green's function we obtain the diagram 1 in Fig. 9a. Similarly, every irreducible diagram in the series for Σ and Φ acts as the beginning of an infinite series of one-eddy reducible diagrams that renormalize all bare propagators to dressed ones. In Fig. 9 we show all the contributions up to 4'th order of the resulting series. This (very important) step in the theory is available due to two facts: the first is that all the topologically allowed diagrams are present, and the second is that the weight of each fragment is determined locally by its symmetry properties.

We note that at this point one can state the following rules of how to draw any diagram in the renormalized series for Σ and Φ :

- I. Only diagrams with an even number of vertices appear.
- II. The series for Σ and Φ contains all the topologically allowed diagrams made of $2n$ vertices with one straight and two wavy legs. The difference is that the diagrams for Σ must have an entry with wavy line and an exit with a straight line, whereas diagrams for Φ have two exits with straight lines.
- III. One needs to exclude all the one-eddy reducible diagrams, and also all diagrams that include closed loops of Green's functions. The latter are zero by causality. They never appear in the method of derivation discussed above, but they do appear in the path integral formulation that is discussed in Section 4. They vanish also there, of course. From these properties it follows that the diagrams for Σ have a unique principal path, and that the diagrams for Φ have a principal cross section.

IV. The coefficient in front of a diagram is determined by the symmetry properties. Every flip of legs that leaves the diagram invariant contributes a factor of $1/2$. However, the

one-eddy irreducible diagrams for Σ cannot have any element of symmetry, and therefore all their weights are unity. The irreducible diagrams for F can have at most one element of symmetry, and they will have a weight of $1/2$. Examples are diagrams 1,5 and 6 in Fig. 9b.

We can show now that the effective coupling constant is of the order of unity. First we discuss how many correlators, propagators and vertices appear in a $2n$ 'th order diagram for Σ and Φ . In a symbolic fashion we can write that

$$\Sigma_{2n} \sim \Sigma_2 \Lambda^{n-1}, \quad \Sigma_2 \sim (\Gamma^2 GF); \quad (3.9)$$

$$\Phi_{2n} \sim \Phi_2 \Lambda^{n-1}, \quad \Phi_2 \sim \Gamma^2 F^2 \quad (3.10)$$

where the new expansion parameter Λ is of the order of

$$\Lambda \sim \Gamma^2 G^2 F. \quad (3.11)$$

To estimate the order of magnitude of Λ we notice that G , according to the Dyson equation (3.4), is of the order of Σ^{-1} . Using this in (3.11) we get

$$\Lambda \sim \frac{\Gamma^2 GF}{\Sigma} \sim \frac{\Gamma^2 GF}{\Gamma^2 GF} \sim 1. \quad (3.12)$$

where Eq. (3.9) has been used. We see that the line-renormalization has shifted our expansion parameter from the order of Re to the order of 1.

At this point one usually considers the possibility of vertex renormalization. In our context this can be achieved by looking at the 2-eddy reducible fragments that can be cut from the bulk by severing three legs. It will turn out that our perturbation series has the deeply non-trivial property that that this step is not needed in the final presentation of the theory. This important issue is discussed further in [21].

We thus end with the Wyld equation which can be rewritten as

$$\begin{aligned} \mathbf{F}(x, x') = \mathbf{G}(x, x_1) * \left[\langle \mathbf{f}(x_1) \mathbf{f}(x_2) \rangle \right. \\ \left. + \langle \phi(x_1) \phi(x_2) \rangle + \Phi(x_1, x_2) \right] * \mathbf{G}(x_2, x') \end{aligned} \quad (3.13)$$

where we have made use of the fact that the thermal noise \mathbf{f} is uncorrelated with the stirring force ϕ . We are going to seek a solution of (3.13) for which the energy of the turbulent motion per mode is much larger than the order of $k_B T$. For such solutions the effect of the thermal noise on the observed statistics of the velocity fluctuations will be negligible, and we can omit $\langle \mathbf{f}(x_1) \mathbf{f}(x_2) \rangle$ from (3.13) with impunity. On the other hand, the role of the stirring force $\langle \phi(x_1) \phi(x_2) \rangle$ can be very important. In general the observed statistics depends on how the fluid is stirred. The choice of stirring that models the boundary condition of experimental turbulence is discussed in [16] after performing some of the analysis on the operators Σ and Φ .

The intuitive understanding of the Wyld equation is also straightforward. From the equation of motion (2.10), written schematically as

$$\mathbf{u} = \frac{1}{[\partial/\partial t - \nu \nabla^2]} \{ -[\mathbf{u} \cdot \nabla] \mathbf{u} + \tilde{\mathbf{f}} \}, \quad (3.14)$$

we see that the nonlinear term $[\mathbf{u} \cdot \nabla] \mathbf{u}$ can be understood as an “additional noise” in the equation of motion. It is natural to expect that the double correlator of the forcing will have a nonlinear contribution of the type

$$\begin{aligned} & \langle \tilde{\mathbf{f}}(\mathbf{r}_1, t_1) \tilde{\mathbf{f}}(\mathbf{r}_2, t_2) \rangle_{\text{NL}} \\ & \sim \langle [\mathbf{u}(\mathbf{r}_1, t_1) \cdot \nabla_1] \mathbf{u}(\mathbf{r}_1, t_1) [\mathbf{u}(\mathbf{r}_2, t_2) \cdot \nabla_2] \mathbf{u}(\mathbf{r}_2, t_2) \rangle. \end{aligned} \quad (3.15)$$

Indeed, the mass operator $\Phi_{\alpha\beta}(\mathbf{r}, \mathbf{r}', t - t')$ can be written exactly as

$$\begin{aligned} & \Phi_{\alpha\beta}(\mathbf{r}, \mathbf{r}', t - t') \\ & = \frac{\partial}{\partial r_\gamma} \frac{\partial}{\partial r'_\delta} F_{\alpha\gamma\beta\delta}(\mathbf{r}, \mathbf{r}, \mathbf{r}', \mathbf{r}', t, t, t', t'), \end{aligned} \quad (3.16)$$

where $F_{\alpha\gamma\beta\delta}$ is the fourth order correlation of \mathbf{u} . Thus Eq.(3.8) can be understood as the result of squaring Eq.(3.14) and averaging, up to the dressing of the Green’s functions. The content of the Wyld diagrammatics is the dressing of the bare Green’s function that appears in Eq.(3.14), and the representation of the fourth order $F_{\alpha\gamma\beta\delta}$ in terms of second order $F_{\alpha\beta}$. The dressing of the Green’s function appears from the cross terms between $[\mathbf{u} \cdot \nabla] \mathbf{u}$ and $\tilde{\mathbf{f}}$ in (3.14). Note that the analytic form of the $\Phi_{\alpha\beta}$ in the 1-loop order, diagram 1 in Fig. 9b, follows directly from the Gaussian decomposition of $F_{\alpha\gamma\beta\delta}$.

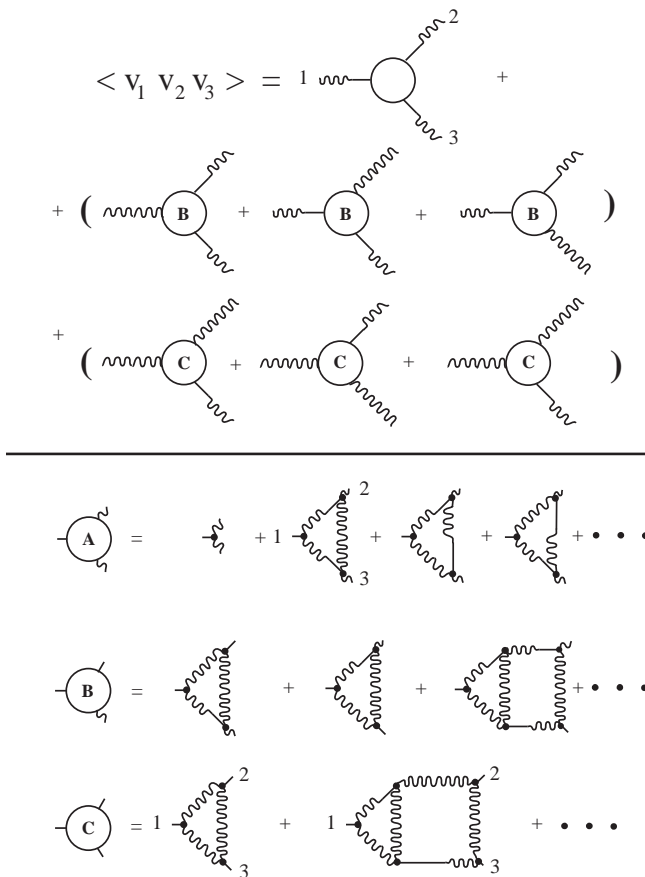


FIG. 10. Diagrammatic representation of the 3-point velocity correlator. Panel (a): There are 3 types of dressed vertices. Panel (b): The diagrammatic expansion for the three vertices appearing in (a). The expansion is in terms of dressed propagators and bare vertices, and we show all the diagrams up to fifth order in the bare vertex.

F. 3-point and higher order velocity correlation functions

To calculate the n -point velocity correlation function we need to take n trees from Fig. 2 and average their product. Diagrammatically it means that we pair branches in all the possible ways, and glue. Next we need to resum all the unlinked diagrams (that sum up to zero), and all the weakly linked diagrams (with the body defined as the structure having n entries) which also give zero contribution. Next we perform a line-renormalization. The procedure is identical to the one described above, and we leave the details to the interested reader. The final result for the 3-point correlation function is shown in Fig. 10. There appear three types of vertices that we denote as A, B and C. Their diagrammatic series is

$$\partial \mathbf{u} / \partial t + (\mathbf{u} \cdot \nabla) \mathbf{u} - \nu \nabla^2 \mathbf{u} - \nabla p = \tilde{\mathbf{f}}, \quad (4.1)$$

with the same properties of the random force $\tilde{\mathbf{f}}$. As before, we need to find the statistical quantities by averaging over all the realizations of the random force $\tilde{\mathbf{f}}$.

Introduce the Navier Stokes functional of \mathbf{u} , $\mathcal{N}\{\mathbf{u}(x)\}$ as

$$\mathcal{N}\{\mathbf{u}(x)\} \equiv \partial \mathbf{u} / \partial t + (\mathbf{u} \cdot \nabla) \mathbf{u} - \nu \nabla^2 \mathbf{u} - \nabla p. \quad (4.2)$$

Given any functional of \mathbf{u} , say $\mathcal{M}\{\mathbf{u}(x)\}$, we can calculate its value for a given realization of \mathbf{u} which in turn is determined by some realization of the random force $\tilde{\mathbf{f}}$. This is done using the formal solution of Eqs. (4.1)–(4.2)

$$\mathbf{u}(x) = \mathcal{N}^{-1}\{\tilde{\mathbf{f}}(x)\} \quad (4.3)$$

according to

$$\mathcal{M}\{\mathbf{u}(x)\} = \mathcal{M}\{\mathcal{N}^{-1}\{\tilde{\mathbf{f}}(x)\}\}. \quad (4.4)$$

The RHS of this equation can be rewritten in the equivalent form

$$\begin{aligned} & \mathcal{M}\{\mathcal{N}^{-1}\{\tilde{\mathbf{f}}(x)\}\} \\ &= \int \mathcal{M}\{\mathbf{u}(x)\} \delta[\mathbf{u}(x) - \mathcal{N}^{-1}\{\tilde{\mathbf{f}}(x)\}] D\mathbf{u}(x). \end{aligned} \quad (4.5)$$

Here the functional integration is interpreted as the continuum limit

$$\int D\mathbf{u}(x) = \lim_{m \rightarrow \infty} \prod_{i=1}^M \int d^3 u(x_i) \delta[\nabla \cdot \mathbf{u}(x_i)], \quad (4.6)$$

where $\{x_i\} = \{r_i, t_i\}$ and i runs over a discrete space-time grid and M is the total number of points in the 4-dimensional grid. The delta function $\delta[\nabla \cdot \mathbf{u}(x_i)]$ limits the integration to divergenceless contributions. The delta functional in (4.5) is defined as the continuum limit

$$\begin{aligned} & \delta[\mathbf{u}(x) - \mathcal{N}^{-1}\{\tilde{\mathbf{f}}(x)\}] \\ &= \lim_{M \rightarrow \infty} \prod_{i=1}^M \delta[\mathbf{u}(x_i) - \mathcal{N}^{-1}\{\tilde{\mathbf{f}}(x_i)\}]. \end{aligned} \quad (4.7)$$

Note that Eq. (4.5) is but a cumbersome generalization to the continuum of the obvious equation

$$f(x) = \int f(y) \delta(x - y) dy. \quad (4.8)$$

Remembering that

$$\delta[g^{-1}(y) - x] = (dg/dx)\delta[g(x) - y], \quad (4.9)$$

one may generalize to the continuum limit according to

$$\delta[\mathbf{u}(x) - \mathcal{N}^{-1}\{\tilde{\mathbf{f}}(x)\}] = J\{\mathbf{u}\}\delta[\mathcal{N}\{\mathbf{u}(x)\} - \tilde{\mathbf{f}}(x)], \quad (4.10)$$

where the Jacobian $J\{\mathbf{u}\}$ is given by

$$J\{\mathbf{u}\} = \det \left| \frac{\delta \mathcal{N}_\alpha\{\mathbf{u}(x)\}}{\delta u_\beta(y)} \right|. \quad (4.11)$$

On the grid this Jacobian is the determinant of the $3M \times 3M$ matrix

$$\begin{aligned} & \frac{\delta \mathcal{N}_\alpha\{\mathbf{u}(x_i)\}}{\delta u_\beta(x_j)} \\ &= \left\{ \delta_{\alpha\beta} \left[\frac{\partial}{\partial t} + (\mathbf{u} \cdot \nabla) - \nu \nabla^2 \right] + \partial_\beta u_\alpha \right\} \delta(x_i - x_j). \end{aligned} \quad (4.12)$$

In the Appendix we demonstrate that this determinant is unity. Thus Eq.(4.4) for \mathcal{M} at a given realization of $\tilde{\mathbf{f}}$ can be rewritten as

$$\mathcal{M}\{\mathbf{u}(x)|\tilde{\mathbf{f}}(x)\} = \int \mathcal{M}\{\mathbf{u}'(x)\}\delta[\mathcal{N}\{\mathbf{u}'(x)\} - \tilde{\mathbf{f}}(x)]D\mathbf{u}'(x). \quad (4.13)$$

Next we need to consider the average of \mathcal{M} with respect to the realizations of \mathbf{u} , (which in turn are determined by the realizations of $\tilde{\mathbf{f}}$). As in the Wyld approach, it will be assumed here that $\tilde{\mathbf{f}}$ has Gaussian statistics. The average of any functional $\mathcal{P}\{\tilde{\mathbf{f}}\}$ can be written as the Gaussian functional integral

$$\begin{aligned} \langle \mathcal{P}\{\tilde{\mathbf{f}}\} \rangle &= \frac{1}{Z_1} \int D\tilde{\mathbf{f}}(x) \mathcal{P}\{\tilde{\mathbf{f}}\} \\ &\times \exp \left[-\frac{1}{2} \int \tilde{f}_\alpha(x) D_{\alpha\beta}^{-1}(x-y) \tilde{f}_\beta(y) dx dy \right]. \end{aligned} \quad (4.14)$$

The covariance matrix $D_{\alpha\beta}$ is determined by the condition that for the case $\mathcal{P}\{\tilde{\mathbf{f}}\} = \tilde{f}_\alpha(x)\tilde{f}_\alpha(y)$ Eq.(4.14) would lead to the equation

$$\langle \tilde{f}_\alpha(x)\tilde{f}_\alpha(y) \rangle = D_{\alpha\beta}(x-y). \quad (4.15)$$

The partition sum Z_1 is

$$Z_1 = \int D\tilde{\mathbf{f}}(x) \exp \left[-\frac{1}{2} \int \tilde{f}_\alpha(x) D_{\alpha\beta}^{-1}(x-y) \tilde{f}_\beta(y) dx dy \right]. \quad (4.16)$$

In performing this average for the functional $\mathcal{M}\{\mathbf{u}(x)|\tilde{\mathbf{f}}(x)\}$ of (4.13) it is convenient to rewrite the delta functional first in an exponential form such that all the \tilde{f} factors appear in the exponential. We use the representation of the 1-dimensional delta function

$$\delta(z) = \int_{-\infty}^{\infty} \frac{dp}{2\pi} \exp(-ipz) \quad (4.17)$$

at every point of the grid. Thus

$$\begin{aligned} \delta[\mathcal{N}\{\mathbf{u}(x)\} - \tilde{\mathbf{f}}(x)] &= \lim_{M \rightarrow \infty} \frac{1}{(2\pi)^M} \int \left[\prod_{i=1}^M dp_{\alpha}(x_i) \right] \\ \exp \left\{ i \sum_{i=1}^M p_{\alpha}(x_i) [N_{\alpha}\{\mathbf{u}(x_i)\} - \tilde{f}_{\alpha}(x_i)] \right\} & \end{aligned} \quad (4.18)$$

We average now Eq.(4.13) using the general Gaussian recipe (4.14), representing the delta function as the continuum limit of (4.17). The result reads

$$\begin{aligned} \langle \mathcal{M}\{\mathbf{u}(x)\} \rangle &= \frac{1}{Z_2} \int D\tilde{\mathbf{f}}(x) D\mathbf{u}'(x) D\mathbf{p} \mathcal{M}\{\mathbf{u}'(x)\} \\ &\times \exp \left\{ i \int dx \mathbf{p}(x) \cdot [\mathcal{N}\{\mathbf{u}'(x)\} - \tilde{\mathbf{f}}(x)] \right\} \\ &\times \exp \left\{ -\frac{1}{2} \int \tilde{f}_{\alpha}(x) D_{\alpha\beta}^{-1}(x-y) \tilde{f}_{\beta}(y) dx dy \right\}. \end{aligned} \quad (4.19)$$

We remind the reader that our path integrals are limited to divergenceless contributions, cf. (4.6). In Eq. (4.19) Z_2 is the partition sum which is the RHS of (4.19) without $\mathcal{M}\{\mathbf{u}(x)\}$. Note that it serves to cancel the formally divergent factor $(2\pi)^M$. Also note that \mathbf{p} appears only in scalar products with divergenceless fields, and any projection onto vector fields that are not divergenceless cancels from $D\mathbf{p}$ with the same $D\mathbf{p}$ that appears in Z_2 . It will be convenient to take \mathbf{p} to be divergenceless from the start, by defining $D\mathbf{p}$ similarly to $D\mathbf{u}$ in Eq.(4.6).

We can perform now the Gaussian integration over $D\tilde{\mathbf{f}}$. One way of doing it is to change the $\tilde{\mathbf{f}}$ variables using a similarity transformation that diagonalizes the matrix D , then to perform the Gaussian integral at each space-time point independently, and lastly to rotate back with the similarity transformation. The final result is

$$\begin{aligned} \langle \mathcal{M}\{\mathbf{u}(x)\} \rangle &= \frac{1}{Z} \int D\mathbf{u}'(x) D\mathbf{p} \mathcal{M}\{\mathbf{u}'(x)\} \\ &\times \exp \left\{ i \int p_{\alpha}(x) \mathcal{N}_{\alpha}\{\mathbf{u}'(x)\} dx \right. \\ &\left. - \frac{1}{2} \int p_{\alpha}(x) D_{\alpha\beta}(x-y) p_{\beta}(y) dx dy \right\}. \end{aligned} \quad (4.20)$$

It is quite evident that (4.20) furnishes a starting point for the calculation of any correlation function $\langle \mathbf{u}(x_1) \mathbf{u}(x_2) \cdots \mathbf{u}(x_n) \rangle$. We recall however that the theory calls also for the calculation of the response or the Green's function. We show now that this calculation is also available from Eq.(4.20). To see this imagine that we add to the force $\tilde{\mathbf{f}}$ some external deterministic

component $\mathbf{h}(x)$ that makes $\langle \mathbf{u}(x_1) \rangle$ non-zero. The addition of this component changes $N_\alpha\{\mathbf{u}(x)\}$ in the exponent in (4.20) to $N_\alpha\{\mathbf{u}(x)\} - \mathbf{h}(x)$. Consider now the response (2.33) which in this case can be represented as

$$G_{\alpha\beta}(x_1, x_2) = i \frac{\delta \langle u_\alpha(x_1) \rangle}{\delta h_\beta(x_2)} \Big|_{h \rightarrow 0}. \quad (4.21)$$

For a finite \mathbf{h}

$$\begin{aligned} \langle u_\alpha(x_1) \rangle &= \frac{1}{Z} \int D\mathbf{u}(x) D\mathbf{p} u_\alpha(x_1) \exp \left\{ i \int p_\beta [\mathcal{N}_\beta\{\mathbf{u}(x)\} \right. \\ &\left. - h_\beta(x)] dx - \frac{1}{2} \int p_\alpha(x) D_{\alpha\beta}(x-y) p_\beta(y) dx dy \right\}. \end{aligned} \quad (4.22)$$

Using this we can compute (4.21):

$$\begin{aligned} G_{\alpha\beta}(x_1, x_2) &= \frac{1}{Z} \int D\mathbf{u}(x) D\mathbf{p} u_\alpha(x_1) p_\beta(x_2) \\ &\times \exp \left\{ i \int p_\beta(x) [\mathcal{N}_\beta\{\mathbf{u}(x)\}] dx \right. \\ &\left. - \frac{1}{2} \int p_\alpha(x) D_{\alpha\beta}(x-y) p_\beta(y) dx dy \right\} = \langle u_\alpha(x_1) p_\beta(x_2) \rangle. \end{aligned} \quad (4.23)$$

In the same way one can compute non-linear response functions like

$$\begin{aligned} G_{\text{NL}}(x_1, x_2, x_3) & \\ \equiv - \frac{\delta^2 \langle u_\alpha(x_1) \rangle}{\delta h_\beta(x_2) \delta h_\gamma(x_3)} \Big|_{h \rightarrow 0} &= \langle u_\alpha(x_1) p_\beta(x_2) p_\gamma(x_3) \rangle \end{aligned} \quad (4.24)$$

etc. It is obvious that every additional functional derivative will appear as another factor of \mathbf{p} in the correlator. In general it is useful to introduce the generating functional

$$Z(\mathbf{l}, \mathbf{m}) \equiv \left\langle \exp \int dx [\mathbf{u}(x) \cdot \mathbf{l}(x) + \mathbf{p}(x) \cdot \mathbf{m}(x)] \right\rangle. \quad (4.25)$$

All the needed statistical averages can be obtained as a functional derivative of $Z(\mathbf{l}, \mathbf{m})$, taken at $\mathbf{l} = \mathbf{m} = 0$, for example

$$\langle u_\alpha(x_1) u_\beta(x_2) \rangle = \frac{\delta^2 Z(\mathbf{l}, \mathbf{m})}{\delta l_\alpha(x_2) \delta l_\beta(x_2)} \quad (4.26)$$

$$\langle u_\alpha(x_1) u_\beta(x_2) u_\gamma(x_3) \rangle = \frac{\delta^3 Z(\mathbf{l}, \mathbf{m})}{\delta l_\alpha(x_2) \delta l_\beta(x_2) \delta l_\gamma(x_3)}, \quad (4.27)$$

etc. Similarly one can compute any kind of Green's function. For example,

$$G_{\alpha\beta}(x_1, x_2) = \frac{\delta^2 Z(\mathbf{l}, \mathbf{m})}{\delta l_\alpha(x_2) \delta m_\beta(x_2)}, \quad (4.28)$$

$$G_{\text{NL}}(x_1, x_2, x_3) = \frac{\delta^3 Z(\mathbf{l}, \mathbf{m})}{\delta l_\alpha(x_2) \delta l_\beta(x_2) \delta m_\gamma(x_3)}, \quad (4.29)$$

$$i \frac{\delta \langle u_\alpha(x_1) u_\beta(x_2) \rangle}{\delta h_\gamma(x_3)} = \frac{\delta^3 Z(\mathbf{l}, \mathbf{m})}{\delta l_\alpha(x_2) \delta l_\beta(x_2) \delta m_\gamma(x_3)}, \quad (4.30)$$

etc. Finally we express the generating functional $Z(\mathbf{l}, \mathbf{m})$, with the help of Eq.(4.20), in the form of a functional integral:

$$Z(\mathbf{l}, \mathbf{m}) = \frac{1}{Z} \int D\mathbf{u}(x) D\mathbf{p}(\mathbf{x}) \quad (4.31)$$

$$\times \exp \left\{ iI + \int dx [\mathbf{u}(x) \cdot \mathbf{l}(x) + \mathbf{p}(x) \cdot \mathbf{m}(x)] \right\} .$$

The quantity I is referred to as the effective action, and for future work it is useful to divide into two parts, the one quadratic and the other triadic in the field \mathbf{p} and \mathbf{u} :

$$I = I_0 + I_{\text{int}} , \quad (4.32)$$

$$I_0 = \int dx \left[p_\alpha \frac{\partial u_\alpha}{\partial t} - \nu p_\alpha \nabla^2 u_\alpha \right] + \frac{i}{2} \int p_\alpha(x) D_{\alpha\beta}(x-y) p_\beta(y) dx dy , \quad (4.33)$$

$$I_{\text{int}} = -i \int dx p_\alpha(x) u_\beta(x) \partial_\beta u_\alpha(x) \quad (4.34)$$

$$= \frac{1}{2} \int \frac{dq_1 dq_2 dq_3}{(2\pi)^{12}} p_\alpha \Gamma_{\alpha\beta\gamma}(q, q_1, q_2) u_\beta(q_2) u_\gamma(q_3)$$

The last line follows from the definition of the vertex in the q representation, see Eq. (2.22). Note that we did not display a transverse projector in the expression of I_{int} . The reason is that the definition (4.6) restricts anyway the integration to divergenceless fields.

Finally, we introduce also the bare generating functional which is (4.31) when $I = I_0$,

$$Z_0(\mathbf{l}, \mathbf{m}) = \frac{1}{Z_0} \int D\mathbf{u}(x) D\mathbf{p} \quad (4.35)$$

$$\times \exp \left\{ iI_0 + \int dx [\mathbf{u}(x) \cdot \mathbf{l}(x) + \mathbf{p}(x) \cdot \mathbf{m}(x)] \right\}$$

This bare generating functional is used in the formulation of the perturbative expansion. We will first use it to evaluate the bare propagators.

C. The evaluation of the bare propagators

It is convenient to change the variables in I_0 from $\mathbf{p}(x)$ and $\mathbf{u}(x)$ to $\mathbf{p}(\mathbf{k}, \omega)$ and $\mathbf{u}(\mathbf{k}, \omega)$, which are defined according to Eq. (2.19). The Jacobian of the transformation (which is formally a divergent constant) cancels with the partition sum:

$$I_0 = \int \frac{dq}{(2\pi)^4} p_\alpha(q) [-i\omega + \nu k^2] u_\alpha(-q) + \frac{1}{2} \int \frac{dq}{(2\pi)^4} p_\alpha(q) D_{\alpha\beta}(q) p_\beta(-q) \quad (4.36)$$

where we remind the reader that $q \equiv (\mathbf{k}, \omega)$.

The bare propagators are computed from $Z_0(\mathbf{l}, \mathbf{m})$ which in this presentation is written as

$$Z_0(\mathbf{l}, \mathbf{m}) = \frac{1}{Z_0} \int D\mathbf{u}(q) D\mathbf{p}(q) \quad (4.37)$$

$$\times \exp \left\{ iI_0 + \int \frac{dq}{(2\pi)^4} [\mathbf{u}(q) \cdot \mathbf{l}(-q) + \mathbf{p}(q) \cdot \mathbf{m}(-q)] \right\} .$$

This functional integral can be computed explicitly. Since we have no mixture of different q 's in the exponent, the exponential can be computed (on the grid) as the product of exponentials. The functional integration is represented as a product of integrals, each one for one discrete q and $-q$:

$$\int D\mathbf{u}(q) = \prod_{q>0} \int du(q) du(-q) .$$

Computing the resulting Gaussian integrals, and using the expression of the bare Green's function (2.16), we end up with

$$Z_0(\mathbf{l}, \mathbf{m}) \quad (4.38)$$

$$= \exp \left\{ \int \frac{dq}{(2\pi)^4} \left[\frac{1}{2} l_\alpha(-q) G_{\alpha\beta}^0(q) D_{\beta\gamma}(q) G_{\gamma\delta}^{0*}(q) l_\delta(-q) \right. \right.$$

$$\left. \left. + G_{\alpha\beta}^0(q) l_\alpha(-q) m_\beta(-q) \right] \right\} .$$

We can check that this zeroth order generating functional gives the same results as the zeroth order quantities defined in the direct perturbation theory. In computing the statistical quantities from (4.38) we use the general property of functional differentiation

$$\frac{\delta l_\alpha(q)}{\delta l_\beta(q')} = (2\pi)^4 \delta(q - q') \delta_{\alpha\beta} . \quad (4.39)$$

and the symmetry of the bare Green's function $G_{\alpha\beta}^0(q) = -G_{\alpha\beta}^{0*}(-q)$ [cf. Eq.(2.16)]. For example, defining the velocity correlation function in q -representation, $F_{\alpha\beta}(q)$, according to

$$\langle u_\alpha(q) u_\beta(q') \rangle = (2\pi)^4 \delta(q + q') F_{\alpha\beta}(q) , \quad (4.40)$$

we compute its bare value $\langle u_\alpha(q) u_\beta(q') \rangle^0$ as

$$\langle u_\alpha(q) u_\beta(q') \rangle^0 = \frac{\delta^2 Z_0(\mathbf{l}, \mathbf{m})}{\delta l_\alpha(-q) \delta l_\beta(-q')} . \quad (4.41)$$

In other words, we find

$$F_{\alpha\beta}^0(q) = G_{\alpha\gamma}^0(q)D_{\gamma\delta}(q)G_{\delta\beta}^*(q) . \quad (4.42)$$

Similarly, defining the Green's function in q -representation as

$$\begin{aligned} (2\pi)^4\delta(q + q')G_{\alpha\beta}(q) \\ = i\frac{\delta\langle u_\alpha(q)\rangle}{\delta h_\beta(q')} \Big|_{h\rightarrow 0} = \langle u_\alpha(q)p_\beta(q')\rangle . \end{aligned} \quad (4.43)$$

Since

$$\langle u_\alpha(q)p_\beta(q')\rangle^0 = \frac{\delta^2 Z_0(\mathbf{l}, \mathbf{m})}{\delta m_\alpha(-q)\delta l_\beta(-q')} , \quad (4.44)$$

we get trivially that

$$\langle u_\alpha(q)p_\beta(q')\rangle^0 = (2\pi)^4\delta(q + q')G_{\alpha\beta}^0(q) .$$

We see that this theory generates the same zeroth order propagators as the direct perturbation expansion of Section II. Note however that there exists an apparent additional propagator here which is absent in II, which is $\langle p_\alpha(q)p_\beta(q')\rangle$. However, the zeroth order $\langle p_\alpha(q)p_\beta(q')\rangle^0$ is zero. This follows from the fact that $Z_0(\mathbf{l}, \mathbf{m})$ does not have a term quadratic in \mathbf{m} in the exponent. We shall show later that it is zero to all orders.

Next we show that the statistics inherited from $Z_0(\mathbf{l}, \mathbf{m})$ are Gaussian statistics. The exponent contained in $Z_0(\mathbf{l}, \mathbf{m})$ can be expanded as

$$\begin{aligned} Z_0(\mathbf{l}, \mathbf{m}) = 1 + \int \frac{dq}{(2\pi)^4} \left[\frac{1}{2}l_\alpha(-q)F_{\alpha\beta}^0(q)l_\beta(q)l_\beta(-q) \right. \\ \left. + l_\alpha(-q)G_{\alpha\beta}^0(q)m_\beta(-q) \right] \\ + \frac{1}{2} \left\{ \int \frac{dq}{(2\pi)^4} \left[\frac{1}{2}l_\alpha(-q)F_{\alpha\beta}^0(q)l_\beta(-q) \right. \right. \\ \left. \left. + l_\alpha(-q)G_{\alpha\beta}^0(q)m_\beta(-q) \right] \right\}^2 + \dots \\ + \frac{1}{n!} \left\{ \int \frac{dq}{(2\pi)^4} \left[\frac{1}{2}l_\alpha(-q)F_{\alpha\beta}^0(q)l_\beta(-q) \right. \right. \\ \left. \left. + l_\alpha(-q)G_{\alpha\beta}^0(q)m_\beta(-q) \right] \right\}^n + \dots \end{aligned} \quad (4.45)$$

Clearly, if we take an odd number of derivatives with respect to l_α , and then send \mathbf{l} and \mathbf{m} to zero, the result vanishes. On the other hand, if we take $2n$ derivatives, and then send \mathbf{l} and \mathbf{m} to zero, only the contributions coming from the n -th power of the integral survive. The answer will be proportional to $[F^0]^n$ with n delta functions. The number of terms will be $2n!/n!2^n$ which is precisely the $(2n - 1)!!$ number of terms expected in the Gaussian statistics (cf. Sect. II C). Note that we have Gaussian statistics also for the field \mathbf{p} .

Instead of looking at the correlation functions, one can study the cumulants. These of course need to vanish beyond the lowest order. An immediate way to obtain the cumulants is to take functional derivatives of $\ln Z_0(\mathbf{l}, \mathbf{m})$ instead of $Z_0(\mathbf{l}, \mathbf{m})$ itself. Obviously,

$$\ln Z_0(\mathbf{l}, \mathbf{m}) = \int \frac{dq}{(2\pi)^4} \quad (4.46)$$

$$\times \left[\frac{1}{2} l_\alpha(-q) F_{\alpha\beta}^0(q) l_\beta(-q) + l_\alpha(-q) G_{\alpha\beta}^0(q) m_\beta(-q) \right].$$

Only the second derivative with respect to \mathbf{l} survives here, giving us only the bare 2-point propagators $F_{\alpha\beta}^0$ and $G_{\alpha\beta}^0$ as the non-vanishing cumulants, as is required for Gaussian statistics.

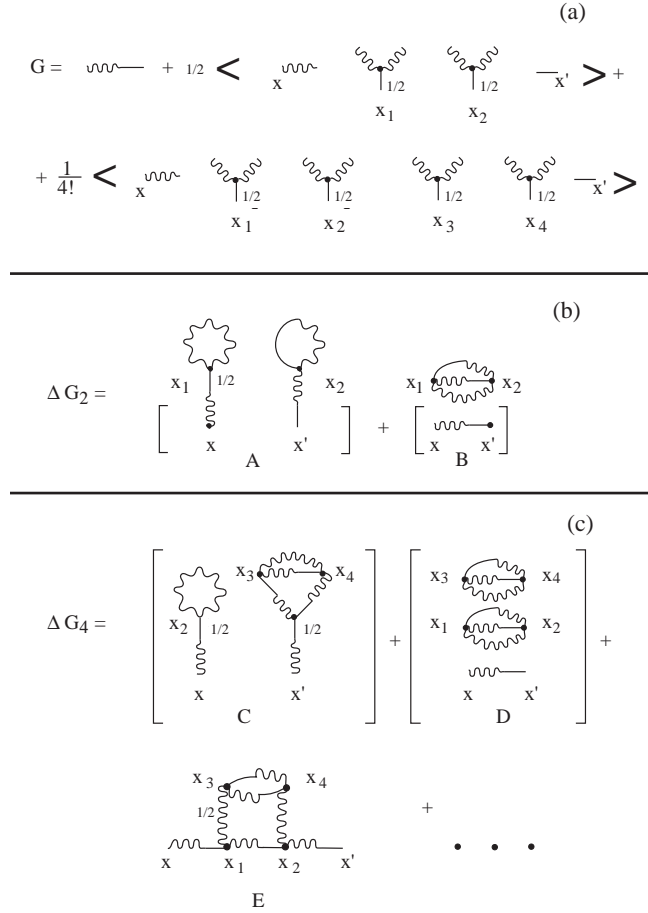


FIG. 12. The graphic representation of Eq.(4.50). Panel (a): The bare, the second order and the fourth order terms. Panel (b): All the diagrams up to order Γ^2 and (c) representative diagrams of order Γ^4 that did not appear in the Wyld diagrammatic series in Fig. 5. All these new diagrams vanish.

D. Diagrammatic expansion

We return to the generating functional $Z(\mathbf{l}, \mathbf{m})$ of Eq.(4.31) and write now the propagator $F_{\alpha\beta}$ and $G_{\alpha\beta}$ as

$$\begin{aligned} F_{\alpha\beta}(x, x') &= \langle u_\alpha(x)u_\beta(x') \rangle \\ &= \langle u_\alpha(x)u_\beta(x') \exp\{iI_{\text{int}}\} \rangle^0, \end{aligned} \quad (4.47)$$

$$\begin{aligned} G_{\alpha\beta}(x, x') &= \langle u_\alpha(x)p_\beta(x') \rangle \\ &= \langle u_\alpha(x)p_\beta(x') \exp\{iI_{\text{int}}\} \rangle^0, \end{aligned} \quad (4.48)$$

with iI_{int} as defined as [cf. (2.18) and (4.34)]

$$iI_{\text{int}} = \frac{1}{2} \int dx p_\alpha(x) \left\{ \Gamma \cdot \frac{\mathbf{u}(x)}{\mathbf{u}(x)} \right\}_\alpha \quad (4.49)$$

Expanding the exponential in (4.47) and (4.48) we find

(a)

$$\begin{aligned} F &= \text{wavy line} + \frac{1}{2} \left\langle \begin{array}{c} \text{wavy line} \\ x \end{array} \begin{array}{c} \text{wavy line} \\ \uparrow 1/2 \\ x_1 \end{array} \begin{array}{c} \text{wavy line} \\ \uparrow 1/2 \\ x_2 \end{array} \begin{array}{c} \text{wavy line} \\ x' \end{array} \right\rangle + \\ &+ \frac{1}{4!} \left\langle \begin{array}{c} \text{wavy line} \\ x \end{array} \begin{array}{c} \text{wavy line} \\ \uparrow 1/2 \\ x_1 \end{array} \begin{array}{c} \text{wavy line} \\ \uparrow 1/2 \\ x_2 \end{array} \begin{array}{c} \text{wavy line} \\ \uparrow 1/2 \\ x_3 \end{array} \begin{array}{c} \text{wavy line} \\ \uparrow 1/2 \\ x_4 \end{array} \begin{array}{c} \text{wavy line} \\ x' \end{array} \right\rangle \end{aligned}$$

(b)

$$\Delta F_2 = \left[\begin{array}{c} \text{star} \\ \uparrow 1/2 \\ x_1 \end{array} \begin{array}{c} \text{wavy line} \\ x \end{array} \right] \begin{array}{c} \text{star} \\ \uparrow 1/2 \\ x_2 \end{array} \begin{array}{c} \text{wavy line} \\ x' \end{array} \Bigg|_A + \left[\begin{array}{c} \text{wavy line} \\ x \end{array} \begin{array}{c} \text{wavy line} \\ \uparrow 1/2 \\ x_1 \end{array} \begin{array}{c} \text{wavy line} \\ \uparrow 1/2 \\ x_2 \end{array} \begin{array}{c} \text{wavy line} \\ x' \end{array} \right] \Bigg|_B$$

(c)

$$\begin{aligned} \Delta F_4 &= \left[\begin{array}{c} \text{star} \\ \uparrow 1/2 \\ x_2 \end{array} \begin{array}{c} \text{wavy line} \\ x \end{array} \begin{array}{c} \text{wavy line} \\ \uparrow 1/2 \\ x_3 \end{array} \begin{array}{c} \text{wavy line} \\ \uparrow 1/2 \\ x_4 \end{array} \begin{array}{c} \text{wavy line} \\ x' \end{array} \right] \Bigg|_C + \left[\begin{array}{c} \text{wavy line} \\ x \end{array} \begin{array}{c} \text{wavy line} \\ \uparrow 1/2 \\ x_1 \end{array} \begin{array}{c} \text{wavy line} \\ \uparrow 1/2 \\ x_2 \end{array} \begin{array}{c} \text{wavy line} \\ \uparrow 1/2 \\ x_3 \end{array} \begin{array}{c} \text{wavy line} \\ \uparrow 1/2 \\ x_4 \end{array} \begin{array}{c} \text{wavy line} \\ x' \end{array} \right] \Bigg|_D + \\ &\left[\begin{array}{c} \text{wavy line} \\ x \end{array} \begin{array}{c} \text{wavy line} \\ \uparrow 1/2 \\ x_1 \end{array} \begin{array}{c} \text{wavy line} \\ \uparrow 1/2 \\ x_2 \end{array} \begin{array}{c} \text{wavy line} \\ \uparrow 1/2 \\ x_3 \end{array} \begin{array}{c} \text{wavy line} \\ \uparrow 1/2 \\ x_4 \end{array} \begin{array}{c} \text{wavy line} \\ x' \end{array} \right] \Bigg|_E + \dots \end{aligned}$$

FIG. 13. The graphic representation of Eq.(4.51). Panel (a): The bare, the second order and the fourth order terms. Panel (b): All the diagrams up to order Γ^2 and representative diagrams of order Γ^4 that did not appear in the Wyld diagrammatic series in Fig. 6. All these new diagrams vanish.

$$G_{\alpha\beta}(x, x') = \sum_n \frac{1}{n!} \langle u_\alpha(x) p_\beta(x') \rangle \times \left\{ \frac{1}{2} \int dx p_\alpha(x) [\Gamma_{\cdot \mathbf{u}(x)}^{\mathbf{u}(x)}]_\alpha \right\}^n \Bigg|^0, \quad (4.50)$$

$$F_{\alpha\beta}(x, x) = \sum_n \frac{1}{n!} \langle u_\alpha(x) p_\beta(x) \rangle \times \left\{ \frac{1}{2} \int dx p_\alpha(x) [\Gamma_{\cdot \mathbf{u}(x)}^{\mathbf{u}(x)}]_\alpha \right\}^n \Bigg|^0, \quad (4.51)$$

Such an expansion contains products of the fields \mathbf{u} and \mathbf{p} averaged over the Gaussian ensemble. As explained above, only products of $\langle u_\alpha(x) p_\beta(x') \rangle^0$ and $\langle u_\alpha(x) u_\beta(x') \rangle^0$ can appear in such a series. (Remember that $\langle p_\alpha(x) p_\beta(x') \rangle^0 = 0$). As done in chapter II, the procedure of computing the averages can be represented diagrammatically by pairing all the allowed pairs of fields and gluing. The needed graphic notation is the same as the one shown in Fig. 1. The field \mathbf{u} is represented by a short wavy line, the field \mathbf{p} by a short straight line, and now it is obvious why the double correlator is represented by a twice long wavy line. Also, the notation for the Green's function becomes natural now, being a correlator of \mathbf{u} and \mathbf{p} . In addition, the notation for the vertex as a dot connecting one straight and two wavy tails becomes apparent in Eqs.(4.50) and (4.51).

The diagrams that are obtained from Eqs.(4.50) and (4.51) are shown in Figs. 12a and 13a respectively. Upon pairing all the possible pairs and gluing, we get exactly the diagrams appearing in Figs. 5a and 6a respectively, and in addition we get the diagrams appearing in panels b and c of Figs. 12 and 13. These additional diagrams, that are denoted here as ΔG_2 , ΔG_4 , ΔF_2 and ΔF_4 respectively, do not appear in the diagrammatic expansion leading to Figs. 5 and 6. However, it is easy to see that they are all zero. The diagram A in 12b contains one term which is a diagram for $\langle \mathbf{u} \rangle$ and another one which represents a contribution to $\langle \mathbf{p} \rangle$. The latter contains a frequency integral over G^0 , which is $-i/2$. However the vertex Γ in front of this contains a factor of \mathbf{k} which is odd in the \mathbf{k} -integration. Therefore the diagram vanishes. The diagrams B, C, D and E in 12b,c contain closed loops of Green's functions. Such loops vanish because of causality: in t -representation only $t = 0$ is allowed for the Green's function in a closed loop, and thus the integral over time has a contribution only from a single point, and it vanishes.

Next we argue that this phenomenon is general: all the diagrams that do not appear in Wyld's expansion are zero. These diagrams are either unlinked (like all the diagrams in Fig. 12 except for E) or linked to the body via wavy lines (like E). All these diagrams must have a closed loop of Green's functions. Consider a diagram from the n -th order, in which m vertices, $m \leq n$, form a fragment that is unlinked to the body. Glue the straight line of the first vertex to the wavy line of another. Then either we close the straight line of the second vertex on the wavy line, or we connect it to a wavy line of a third vertex. The first possibility leads to zero due to the argument of diagram A in 12b. In the second possibility we again need to repeat the same option, or to closed with the first vertex. The production of a close loop of Green's functions is inevitable, and these vanish due to causality. Diagrams that are connected only via wavy lines also must have a closed loop of Green's functions for the same reasons.

We thus conclude that the path integral formulation leads to exactly the same diagrams as the Wyld direct perturbative expansion. This fact is not widely recognized. One reason for this is that in Ref. [9] the three types of vertices which appear in this theory were not explicitly discussed. They were first dealt with properly in [10] in which it was stated that the results agree with [9] only to order Γ^3 . We have shown above that the two techniques generate exactly the same (non-zero) diagrams on the naive level, and these can be resummed in exactly the same way. For example, Fig. 6 of Ref [21] was claimed to differ from the Wyld technique, but in fact is identical to the present Fig. 10b which was obtained entirely within the Wyld expansion.

5. SUGGESTIONS FOR FURTHER READING

The material presented in these notes should be sufficient to prepare the student for reading the research papers on the subject of renormalized perturbation theory of turbulence. For the convenience of the interested student we present in this section a brief guided tour through the latest publications of our own group. The next paper to read is [16] in which the Belinicher-L'vov renormalization scheme is used to prove that the theory for the correlation functions and the Green's functions is finite. In other words, it is shown (order by order) that for $\text{Re} \rightarrow \infty$, after the appropriate resummations, all the diagrams converge both in the IR and the UV limits. This fact tells us that there is no length scale available to form dimensionless corrections to the K41 scaling. In [19] the issue of anomalous scaling is discussed. It is shown that there exist anomalous exponents in turbulence, but they appear

in gradient fields and their correlations. Thus for example the dissipation field is anomalous, and its correlation function is strongly renormalized compared with the Gaussian limit. The issue of the effect of the anomalous fields on the structure functions was discussed in [20]. It is argued there that the anomalous fields are subcritical, and that they influence the structure functions only on the level of corrections to scaling. The latter corrections are large, and they disappear only at very large values of Re . We attributed the observed deviations in experiments to these “subcritical” corrections. Two more papers that may be considered are [22] and [23] in which further relations to experiments are discussed. In [23] we discuss which length scale should be used as the renormalization scale in turbulence, i.e the inner scale η or the outer scale L . In [22] one can find an experimental test of some aspects of the new theory, especially some unusual correlation functions between velocity differences and the dissipation field.

ACKNOWLEDGMENTS

We thank Adrienne Fairhall and Volodia Lebedev for their comments on the manuscript. This work has been supported in part by the German-Israeli Foundation and the N. Bronicki fund.

6. APPENDIX: THE JACOBIAN

In this appendix we explain the known fact [17,18] that the Jacobian that appears in Eq.(4.10) is unity. From the definition of the delta function it is obvious that

$$\int D\mathbf{u}(x)\delta[\mathbf{u}(x) - \mathcal{N}^{-1}\{\tilde{\mathbf{f}}(x)\}] = 1 . \quad (6.1)$$

This means that also the functional integral over the RHS of Eq.(4.10) is unity. What we want to prove now is that also the functional integral on the RHS of (4.10) without $J\{\mathbf{u}\}$ is unity:

$$\int D\mathbf{u}(x)\delta[\mathcal{N}\{\mathbf{u}(x)\} - \tilde{\mathbf{f}}(x)] = 1 . \quad (6.2)$$

This will be the first indication that the Jacobian $J\{\mathbf{u}\} = 1$. To accomplish this we will only use the fact that the Navier-Stokes equations are first order in the time derivative:

$$\mathcal{N}\{\mathbf{u}(x)\} = \frac{\partial\mathbf{u}(x)}{\partial t} + \text{NL}\{\mathbf{u}(x)\} . \quad (6.3)$$

The time derivative on the time grid may be represented in the retarded convention

$$\frac{\partial \mathbf{u}_n(\mathbf{r})}{\partial t_n} = [\mathbf{u}_n(\mathbf{r}) - \mathbf{u}_{n-1}(\mathbf{r})]/\tau . \quad (6.4)$$

Using this representation we rewrite (6.2) on the time grid as

$$\int \prod_n D\mathbf{u}_n(\mathbf{r}) \delta[\mathbf{u}_n(\mathbf{r}) + \widetilde{\text{NL}}\{\mathbf{u}_{n-1}(\mathbf{r})\}] . \quad (6.5)$$

We have collected everything except \mathbf{u}_n itself into an operator that was denoted as $\widetilde{\text{NL}}$. It is obvious now that every $D\mathbf{u}_n(\mathbf{r})$ integration yields unity due to the delta function, and finally the result is unity. Next one should prove that the functional integrals (6.1) and (6.2) but with any arbitrary weight functional of \mathbf{u} are also the same. Repeating the same considerations on the time grid furnishes this demonstration with essentially the same ease.

REFERENCES

* L'vov's e-mail: fulvov@wis.weizmann.ac.il.

† Procaccia's e-mail: cfprocac@weizmann.weizmann.ac.il.

- [1] L.F. Richardson. *Weather Prediction by Numeric Process*. Cambridge Univ. Press, Cambridge, 1922.
- [2] Lewis F. Richardson. Atmospheric diffusion shown on a distance neighbor graph. *Proc. R. Soc. Lond. A*, 110:709–737, 1926.
- [3] A. S. Monin and A. M. Yaglom. *Statistical Fluid Mechanics: Mechanics of Turbulence*, volume II. The MIT Press, Cambridge, Mass., 1973.
- [4] A. N. Kolmogoroff. über das logarithmisch normale Verteilungsgesetz dd Dimensionen der Teilchen bei Zerztckelungg. *C. R. (Doklady) Acad. Sc. URSS*, 31:99–101, 1941.
- [5] Uriel Frisch. *Turbulence: The Legacy of A.N. Kolmogorov*. Cambridge University Press, Cambridge, 1995. In press.
- [6] K.R. Sreenivasan and P. Kailasnath. An update on the intermittency exponent in turbulence. *Phys. Fluids A*, 5(2):512–514, 1993.
- [7] R.H. Kraichnan. The structure of isotropic turbulence at very high Reynolds numbers. *J. Fluid Mech.*, 5:497–543, 1959.
- [8] S. A. Orszag. Analytical theories of turbulence. *J. Fluid Mech.*, 41:363–386, 1970.
- [9] H. W. Wyld. Formulation of the theory of turbulence in an incompressible fluid. *Ann. Phys.*, 14:143–165, 1961.
- [10] P. C. Martin, E. D. Siggia, and H. A. Rose. Statistical dynamics of classical systems. *Phys. Rev. A*, 8(1):423–437, July 1973.
- [11] V. E. Zakharov and V. S. L'vov. On statistical description of the nonlinear wave fields. *Quan. Electronics*, 18(10):1084–1097, 1975.
- [12] R. H. Kraichnan. Lagrangian-history closure approximation for turbulence. *Phys. Fluids*, 8:575–598, 1965.
- [13] R.H. Kraichnan. Isotropic turbulence and inertial-range structure. *Phys. Fluids*, 9:1728–1752.

- [14] V. I. Belinicher and V. S. L’vov. A scale-invariant theory of fully developed hydrodynamic turbulence. *Sov. Phys. JETP*, 66:303–313, 1987.
- [15] V. S. L’vov. Scale invariant theory of fully developed turbulence. Hamiltonian approach. *Phys. Rep.*, 207(1):1–47, August 1991.
- [16] V. S. L’vov and I. Procaccia. Exact resummations in the theory of hydrodynamic turbulence. I. The ball of locality and normal scaling. *Phys. Rev. E*, 1995. Submitted.
- [17] C. DeDominics. *J. Physique (Paris)*, 37:C1–247, 1976.
- [18] H.K. Jansen. *Z. Phys. B*, 23:377, 1976.
- [19] V. S. L’vov and I. Procaccia. Exact resummations in the theory of hydrodynamic turbulence. II. A ladder to anomalous scaling. *Phys. Rev. E*, 1995. Submitted.
- [20] V. S. L’vov and I. Procaccia. “Intermittency” in turbulence as intermediate asymptotics to Kolmogorov’41 scaling. *Phys. Rev. Lett.*, 1995. Submitted, E-print in Los-Alamos e-board No 9410002 (1994) chao-dyn@xyz.lanl.gov .
- [21] V. S. L’vov and V. V. Lebedev. Exact relations in the theory of fully developed hydrodynamic turbulence. *Phys. Rev. E*, 47(4):1794–1802, 1993.
- [22] V. S. L’vov and I. Procaccia. Correlator of velocity differences and energy dissipation as element in the subcritical scenario for nonKolmogorov scaling in turbulence. *Europhys. Lett.*, 1995. In press.
- [23] V.S. L’vov and I. Procaccia. Is the fundamental length scale in developed turbulence the inner or the outer scale ? *Phys. Rev. E*, 1995. Submitted